Received: 5 April 2022 | Revised: 9 June 2022 | Accepted: 6 July 2022

DOI: 10.1002/aoc.6821

RESEARCH ARTICLE

Applied Organometallic Chemistry WILEY

Ni(II) complexes with 1,3,2,4-dithiadiphosphetane 2,4-disulfide-based ligands: Structural insights, theoretical studies, and anticancer activities

Elif Bulat[1,2] | **Ertuğrul Gazi Sağlam**[1,2] | **Celal Tuğrul Zeyrek**[3] | **Senem Akkoç**[4,5] | **Yunus Zorlu**[6] | **Hakan Dal**[7]

[1]Department of Chemistry, Yozgat Bozok University, Yozgat, Turkey

[2]Department of Chemistry, Marmara University, İstanbul, Turkey

[3]Department of Medical Services and Techniques, Çankırı Karatekin University, Çankırı, Turkey

[4]Department of Basic Pharmaceutical Science, Süleyman Demirel University, Isparta, Turkey

[5]Faculty of Engineering and Natural Sciences, Bahçeşehir University, Istanbul, 34353, Turkey

[6]Department of Chemistry, Gebze Technical University, Gebze, Turkey

[7]Department of Medical Services and Techniques, Anadolu University, Eskişehir, Turkey

Correspondence
Ertuğrul Gazi Sağlam, Department of Chemistry, Yozgat Bozok University, Yozgat 66900, Turkey; Department of Chemistry, Marmara University, Göztepe, İstanbul 34722, Turkey.
Email: ertugrulgazi.saglam@yobu.edu.tr; egazi@marmara.edu.tr; saglameg@gmail.com

Funding information
Yozgat Bozok Üniversitesi, Grant/Award Number: BAP 6602c-FEN/20-359; Marmara Üniversitesi, Grant/Award Number: BAPKO; Project No: FDK- FDK-2021-10339; Türkiye Bilimsel ve Teknolojik Araştirma Kurumu, ULAKBIM: High Performance and Grid Computing Center (TRUBA; Suleyman Demirel University Research Fund, Grant/Award Number: TSG-2021-8458; Marmara University; Yozgat Bozok University

The first synthesis of 2,4-*bis*(3,4-dimethoxyphenyl)-1,3-dithia-2,4-diphosphetane 2,4-disulfide (SAV-A1 reagent) was achieved. Seven oxo-alkyl esters (HLn) were synthesized thereof. Ni(II) complexes ($[Ni(Ln)_2]$) of these ligands were prepared in ethanol. The structures were identified by spectral studies. Ni(II) complexes were unambiguously determined by X-ray crystallography. In addition, the ligands and their Ni(II) complexes were tested on two different human cancer cell lines, including liver and colon. Moreover, density functional theory (DFT) calculations of the Ni(II) complexes were performed, and the molecular docking studies of these compounds with liver cancer protein, PDB ID: 3WZE and colon cancer antigen proteins, ID 2HQ6 were presented to investigate and predict potential interactions.

KEYWORDS

2,4-diorganyl-1,3,2,4-dithiadiphosphetan-2,4-disulfide, anticancer, density functional theory, dithiophosphonato complexes, perthiophosphonic acid anhydrides

1 | INTRODUCTION

Over the past few decades, the compounds bearing a P_2S_2 moiety are dubbed 2,4-diorganyl-1,3,2,4-dithiadiphosphetane-2,4-disulfide (DTPS, $(RP(S)S)_2$) have attracted much attention, because they serve as the starting material of a series of new organodithiophosphorus compounds.[1–7] The prototype of the DTPSs is the so-called Lawesson reagent.[8] Other analogs, for example, Belleau reagent,[9] Yokoyama reagent,[10] and Davy reagent[11] have been reported afterward (Figure 1).

Lawesson's and Davy's reagents are commercially available,[12] whereas other DTPSs are synthesized as needed. There are three routes for the syntheses of these reagents: the reaction of thiophosphine dichlorides with H_2S[13]; the treatment of the diphosphines with elemental

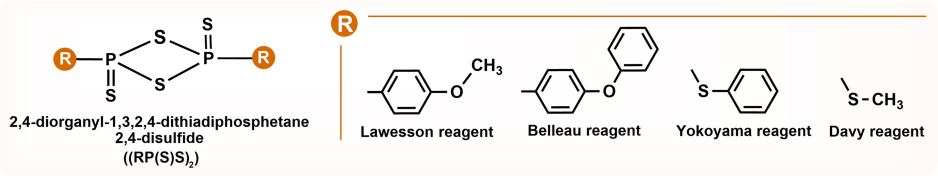

FIGURE 1 Some of the DTPS reagents

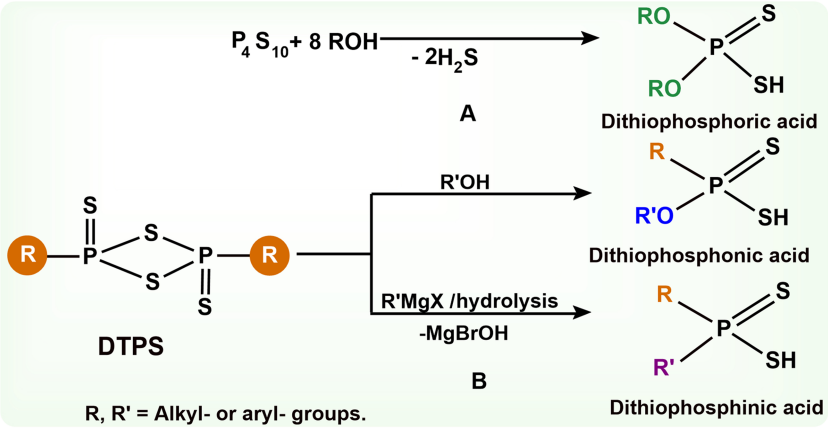

SCHEME 1 The syntheses of dithiophosphonic acids (a) and dithiophosphinic acids (b)

sulfur[14]; and by the reaction of P_4S_{10} with aliphatic or aromatic compounds.[15–17] The last method appears to be superior to the others in that virtually no by-products accompany; the whole process is a single step, and the starting materials are stable against open-air, humidity, and mild heat in terms of the starting materials of other methods.

Organodithiophosphorus compounds include dithiophosphoric-, dithiophosphonic-, and dithiophosphinic acids. Dithiophosphoric acid[18] synthesis requires a different approach, for example, the direct reaction of P_4S_{10} with alcohols (Scheme 1a). Dithiophosphonic- and dithiophosphinic acids are prepared by the reaction of DTPSs with alcohols[19] and Grignard reagents,[20] respectively (Scheme 1b).

Organodithiophosphorus compounds find practical uses in, for example, agriculture (as insecticides and pesticides)[21,22]; industry (as antioxidant-additives for lubricants)[23]; solvent-extraction reagents for metals[24]; flotation agents for mineral ores[25,26]; and medicine (as potential antibiotics, antimicrobial agents, and possible anticancer agents).[27–32] Their use in metal mining is based on the fact that they provide two soft-base type sulfur ligands[33] so as to form a four-ring chelate. Depending on the metal cation, they usually form either four- or six-coordinate complexes.[34–36] Ni(II) complexes are well-known among the four coordinate metal complexes.[37–40]

S-tributylstannyl dithiophosphates and dithiophosphonates were prepared, and the bactericidal activity of S-tributylstannyl dithiophosphates was tested on *Staphylococcus aureus* (ATCC 29213), *Escherichia coli* (ATCC 25922), and *Bacillus cereus*.[41] These compounds tested had more activity towards *B. cereus* than control Nika-Politsid (10 mm) and Slayt (12 mm) with growth inhibition zone of 23–24 mm. In a different study, some Ni(II) complexes of dithiophosphonic acids were synthesized, and their biological activities were tested against *Pseudomonas aeruginosa* (ATCC 27853), *E. coli* (ATCC 25922), and *Acinetobacter baumannii* (ATCC 19606) using disk diffusion method.[42] The results demonstrated that the most sensitive bacterial strains on the compounds tested were gram-negative bacteria, *A. Baumannii*, *E. coli*, and *P. aeruginosa*. Dithiophosphonates and amidodithiophosphonates compounds were synthesized[43] and screened against seven gram-positive bacteria, seven gram-negative bacteria, and three different Methicillin-Resistant *Staphylococcus aureus* (MRSA) strains. The results showed that a compound had potent anti-MRSA activity.

There are few published studies on the cytotoxic activities of dithiophoshorus compounds, let alone on the dithiophosphinic acid[44] and dithiophosphonic acid[45–47] compounds. In contrast, antiproliferative activity studies on dithiophosphoric acid compounds appear to be more frequent.[48] For example, a study by Lowe et al. showed that Pt(II)-dithiophosphoric acid complexes have cytotoxic activity.[49] In another study by Kumar et al., it is reported that some vanadium-based dithiophosphate complexes were active against lung, prostate, and leukemia cancers.[50] These studies obviously need some supporting research to arrive at a more conclusive idea about

the anticancer activity of dithiophoshorus derivatives as a whole.

In this work, we present the synthesis, characterization, and a preliminary trial for the possible uses of a new group of organodithiophosphorus compounds that are prepared from a single starting material, namely, 2,4-*bis*(3,4-dimethoxyphenyl)-1,3-dithia-2,4-diphosphetane 2,4-disulfide (SAV-A1 reagent) (Scheme 2).

The treatment of SAV-A1 reagent with alcohols yielded the dithiophosphonic acids, $HS_2P((C_6H_3(3,4\text{-}CH_3O)_2)(ORn))$; R1 = methyl-; R2 = ethyl-; R3 = n-propyl-; R4 = n-butyl-; R5 = 3-pentyl-; R6 = 3-methyl-1-butyl-; R7 = benzyl. The dithiophosphonic acids are encrypted as HLn and the ligands thereof as Ln with the "n" values following the order given above (between **1** and **7**; see Scheme 3). HLn acids were converted to their ammonium salts (NH_4Ln) by passing dry ammonia through their impure, concentrated benzene solutions. The treatment of NH_4Ln with $NiCl_2.6H_2O$ in ethanol led to the complexes ($[Ni(Ln)_2]$). The structures of the compounds were characterized by spectroscopic methods (mass spectrometry [electrospray ionization (ESI)], Fourier transform ınfrared [FT-IR] spectroscopy, ^1H-, ^{13}C-, ^{31}P-nuclear magnetic resonance [NMR], and 2D-heteronuclear single quantum coherence (HSQC) techniques (for $[Ni(L6)_2]$), and elemental analysis. All complexes were elucidated by single-crystal X-ray diffraction analyses.

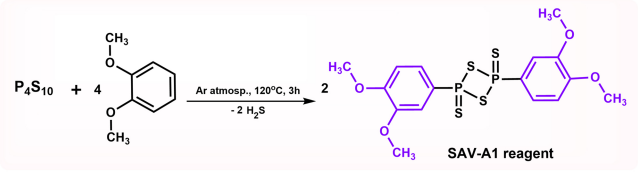

SCHEME 2 Synthesis reaction of SAV-A1 reagent

Quantum mechanical calculations on the ground states of Ni(II) dithiophosphonato complexes have been performed using B3LYP/LANL2DZ/6-31+G(d,p) level, and the optimized geometries were compared with those found by the X-ray diffraction technique. The ground state energy levels, chemical parameters, the orientation of the frontier molecular orbitals (highest occupied molecular orbitals [HOMOs] and lowest unoccupied molecular orbitals [LUMOs]), and molecular potential surfaces (MEPs) of the compounds have been predicted via density functional theory (DFT) in the gas phase. The molecular docking studies (MDSs) of the Ni(II) complexes on the liver cancer protein, PDB ID: 3WZE and colon cancer antigen proteins, ID 2HQ6 have also been investigated to predict potential interactions.

2 | MATERIALS AND METHODS

Reagents, instruments, X-ray data collection and structure refinement procedures, Hirshfeld surface (HS) analysis, computational methods (DFT calculations and molecular docking calculations), general procedure and structural data, in vitro cytotoxic activity studies of the compounds are summarized in the Supporting Information (SI). Analytical procedures, spectroscopic data, and spectra of the compounds are also summarized in SI.

3 | RESULTS AND DISCUSSION

3.1 | Spectroscopic studies

3.1.1 | IR spectra

Selected IR data (cm^{-1}) assignment of vibrational bands for the compounds is given in Table S1. The characteristic $\nu_{N\text{-}H}$ stretching bands of the ligands appear

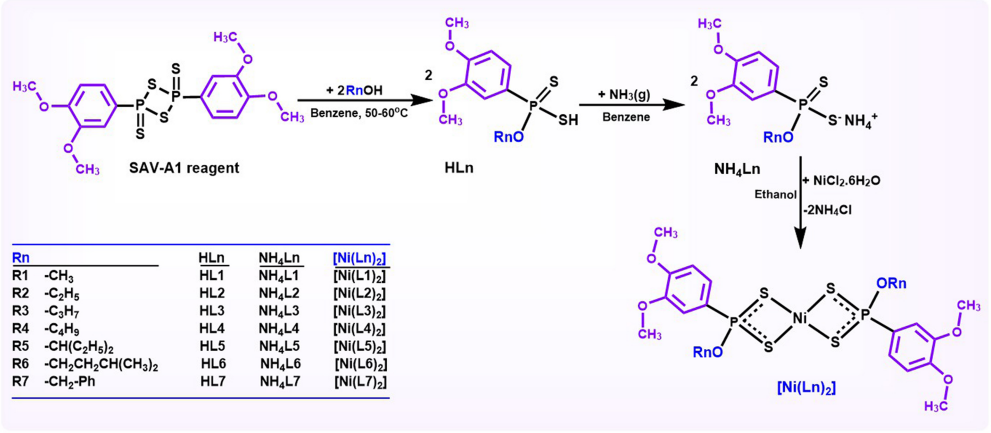

Rn	HLn	NH_4Ln	$[Ni(Ln)_2]$
R1 $-CH_3$	HL1	NH_4L1	$[Ni(L1)_2]$
R2 $-C_2H_5$	HL2	NH_4L2	$[Ni(L2)_2]$
R3 $-C_3H_7$	HL3	NH_4L3	$[Ni(L3)_2]$
R4 $-C_4H_9$	HL4	NH_4L4	$[Ni(L4)_2]$
R5 $-CH(C_2H_5)_2$	HL5	NH_4L5	$[Ni(L5)_2]$
R6 $-CH_2CH_2CH(CH_3)_2$	HL6	NH_4L6	$[Ni(L6)_2]$
R7 $-CH_2$-Ph	HL7	NH_4L7	$[Ni(L7)_2]$

SCHEME 3 The syntheses of ligands and their Ni(II) complexes

at 3190–2931 cm^{-1} on IR. These bands disappear on the IR spectra of the complexes proving the substitution of the ammonium group by metal cations. For the ligands, symmetric and asymmetric PS stretching bands ($\nu(PS)_{sym}$ and $\nu(PS)_{asym}$) are observed at 610–544 cm^{-1} and 689–641 cm^{-1}, respectively.[7,41–43,51,52] The IR spectra of the complexes all show two bands in the ranges 562–553 and 663–630 cm^{-1} attributable to the ν_{sym} and ν_{asym} PS stretching vibrations, respectively. The complexes also display Ni-S bands. IR spectral symmetric and asymmetric Ni-S stretching bands ($\nu(Ni\text{-}S)_{sym}$ and $\nu(Ni\text{-}S)_{asym}$) are located at 263–296 and 323–351 cm^{-1}, respectively. IR data reported for similar compounds agree well with our findings.[30,38,53,54]

3.1.2 | Mass spectra

The ESI-MS spectra of the compounds are presented in the SI. Some MS peaks display m/z values that are 23 or 41 units higher than the value corresponding to the m/z of the probably-candidate species. This is attributed to the attachment of sodium or acetonitrile contaminations from the buffer or the solvent. In the MS spectra of the ligands, the peak pertaining to the molecular ion $[M\text{-}NH_4]^+$ is the principal peak. The molecular ion peak is also the principle one in the spectra of the complexes except for those $[Ni(Ln)_2]$ complexes with n = 1, 3, 6, and 7.

3.1.3 | NMR spectroscopy

The starting material, DTPS, is insoluble in the common NMR solvents, so no NMR data were provided for it. The NMR spectra and important NMR data for the ligands and their nickel(II) complexes are presented in Tables S2–S6. The numbering system used for assignments of the protons is also given in Figure S1.

The C_6-***H*** proton in the 3,4-dimethoxyphenyl ring appears as a doublet of doublets due to splittings by the phosphorous ($^3J_{PH}$ = 12.6–14.4 Hz for the ligands and $^3J_{PH}$ = 14.2–15.1 Hz for the complexes) and also by C_5-***H*** proton ($^3J_{HH}$ = 8.2–8.4 Hz for the ligands and $^3J_{HH}$ = 7.8–8.4 Hz for the complexes). Splittings by the other aromatic proton are not observable. The C_2-***H*** proton gives rise to a doublet as it is split by phosphorous ($^3J_{PH}$ = 13.8–14.7 Hz for the ligands and $^3J_{PH}$ = 15.1–15.3 Hz for the complexes). Here again, splittings by distant aromatic protons are below the observable limit. C_5-***H*** proton displays a four-bond coupling to phosphorus ($^4J_{PH}$ = 3.6–3.8 Hz for ligands and $^4J_{PH}$ = 3.3–4.2 Hz for complexes); therefore, this proton also appears as a doublet of doublets. The chemical shifts of the methoxy protons are virtually the same (δ = ~3.6–4.0 ppm in all compounds).

The chemical shifts of the P-O-C_9-***H*** protons in the ligands tend to move to lower fields in the spectra of the corresponding nickel complexes. These protons appear very close to the aromatic ring O-C***H***$_3$ protons on the spectra of the ligands but more distant on those of the complexes because the aromatic ring O-C***H***$_3$ protons are less effected by the complexation. The ***H***-C_{10}-***H*** protons on the ligand $[NH_4L6]$ are typically diastereotopic and remain the same on the spectrum of the corresponding nickel complex.

On the ^{13}C-NMR spectra of the ligands, the nuclei ***C***$_2$ and ***C***$_6$ are split by the phosphorus in the ranges, $^2J_{PC}$ = 14.6–15.0 Hz and 12.2–12.8 Hz, respectively. These values lie in the expected domain.[7] As is the case in many similar structures, the three-bond P-***C*** coupling displayed by the nuclei ***C***$_3$ and ***C***$_5$ ($^3J_{PC}$ = 16.8–17.4 Hz and 16.8–18.3 Hz, respectively) is higher than the two-bond couplings of ***C***$_2$ and ***C***$_6$.

The difference between the ^{13}C NMR spectra of the complexes and those of the corresponding ligands is not worth commenting on.

Proton-decoupled ^{31}P-NMR spectra all the compounds comprise single peaks. The chemical ^{31}P chemical shifts of the ligands are located in the range 103.7–109.6 ppm and those of the complexes in the range 96.3–104.5 ppm, which means that the complex formation causes a shift of δ = ~4–6 ppm to higher fields.

The ambiguity regarding the assignments of ^{1}H- and ^{13}C-NMR peaks of $[Ni(L6)_2]$ complex was dealt with by using HSQC spectra (Figure 2). All the NMR values compare well with the literature reports for similar structures.[53,55–62]

3.2 | Crystallographic descriptions of the Ni(II) complexes

The crystallographic data and refinement details of the data collection for all complexes are given in Table 1. Crystal structures of $[Ni(Ln)_2]$ (n = 1–7) were unambiguously confirmed through single-crystal X-ray diffraction analysis. $[Ni(L1)_2]$, $[Ni(L2)_2]$, $[Ni(L6)_2]$, and $[Ni(L7)_2]$ appear to crystallize in the monoclinic system, whereas $[Ni(L4)_2]$ and $[Ni(L5)_2]$ display a triclinic structure with *P*-1. Unlike other complexes, $[Ni(L3)_2]$ belongs to orthorhombic *Pbca* space group. Whereas the asymmetric unit of most Ni(II) complexes consists of a single molecule, that of $[Ni(L6)_2]$ involves two crystallographically independent compounds.

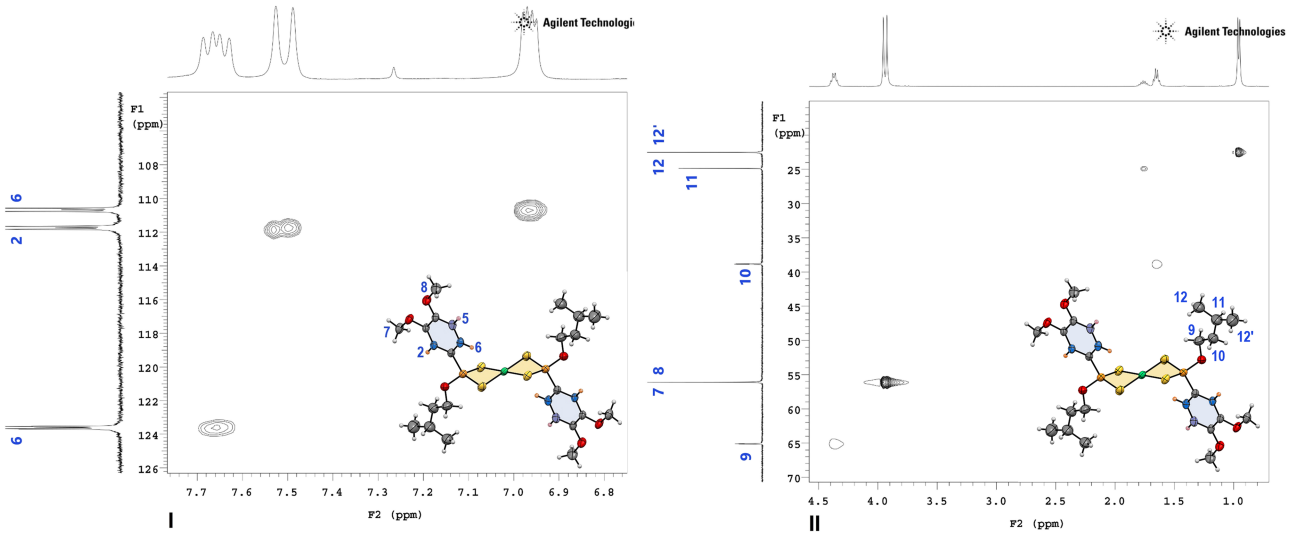

FIGURE 2 Heteronuclear single quantum coherence (HSQC) spectrum (**I**) for the aromatic region and (**II**) for the aliphatic region of $[Ni(L6)_2]$

All the complexes consist of two dithiophosphonate (L) and one crystallographically distinct Ni(II) ions. The numbering figures are depicted in Figures 3a–9a. The Ni(II) ion in each of the complexes has a square planar coordination geometry formed by four sulfur atoms from two dithiophosphonate ligands. In $[Ni(L1)_2]$, $[Ni(L2)_2]$, $[Ni(L3)_2]$, $[Ni(L4)_2]$, and $[Ni(L5)_2]$, four-coordinate τ_4 parameters for Ni(II) are between 0 and 0.037, and it can be considered as ideal square planar geometry.[63] It is worth noting that the dithiophosphonate moieties in $[Ni(L1)_2]$ are in *cis*-configuration with respect to the coordination plane, and similar structures with *cis*-arrangement are very rare in the literature.[64,65] This may be attributed to the relatively less steric hindrance of methyl groups compared with the bulkier alkyl- and aryl- moieties in the other dithiophosphonates.

The selected bond lengths and bond angles are given in Table S7. The Ni—S bond distances in Ni(II) coordination sphere are between 2.2148(13)–2.2311 (12) Å/2.1970–2.3501 Å (Exp./Cal.) for $[Ni(L1)_2]$, 2.2228 (6)–2.2267(6)/2.3480–2.3489 Å (Exp./Cal.) for $[Ni(L2)_2]$, 2.2121(8)–2.2246(8) Å/2.3483–2.3488 Å (Exp./Cal.) for $[Ni(L3)_2]$, 2.2288(6)–2.2318(5) Å/2.3440–2.3482 Å (Exp./Cal.) for $[Ni(L4)_2]$, 2.2261(15)–2.2388(14) Å/2.3440–2.3482 (Exp./Cal.) for $[Ni(L5)_2]$, 2.2217 (11)–2.2294 (9) Å/2.3482–2.3485 Å (Exp./Cal.) for $[Ni(L6)_2]$, and 2.2156(4)–2.2244(4) Å/2.3475–2.3476 Å for $[Ni(L7)_2]$. The S—Ni—S bond angles exhibit almost the same tendency in all complexes and range from 87.84 (5)° to 180.0°/89.325° to 180.0° (Exp./Cal.). As expected, the optimized bond lengths are somewhat longer than the experimental values. These results are not surprising because the optimized results are based on the unpacked isolated molecules, whereas the experimental results are obtained in the solid-state form. The N—S bond distances and S—Ni—S bond angles are compatible with those previously found in dithiophosphonato Ni(II) complexes.[35,40,64–70] The average P—S bond lengths for $[Ni(Ln)_2]$ are typically about 2.0 Å, which shows that π-electron delocalization prevails in the -PS_2 moiety of dithiophosphonates. These values are consistent with the literature reports.[69,71–75] As indicated in Table S8, intermolecular C—H···O hydrogen bonding interactions are to be considered "weak" because the experimental C—H···O distance between the CH groups and O atoms in the dithiophosphonato anions ($d_{(O\cdots H)} \sim 2.52$–$2.72$ Å) is longer than the corresponding van der Waals distances ($r_{vdw}(O) + r_{vdw}(H) = 2.72$ Å), (Figures 3b–9b). On the other hand, the C—H···S hydrogen bonding interactions (corresponding van der Waals distances [$r_{vdw}(S) + r_{vdw}(H) = 3.00$ Å]) were observed only in $[Ni(L1)_2]$, $[Ni(L2)_2]$, and $[Ni(L7)_2]$ (Figures 3d, 4d, and 9c). It is noteworthy that, in all the complexes, the short intermolecular π···π interactions with less than 3.8 Å distance in between are not present. But C—H···π interactions for $[Ni(L1)_2]$, $[Ni(L2)_2]$, $[Ni(L3)_2]$, $[Ni(L5)_2]$, and $[Ni(L7)_2]$ are notable.

In $[Ni(L1)_2]$, the C8—H8C···O5 ($d_{(C8\cdots O5)} = 3.454$ Å) contacts link the molecules to form a hydrogen-bonded dimer (Figure 3b). HS of $[Ni(L1)_2]$ is illustrated in Figure 3c, and the O···H/H···O interactions appear as distinct spikes in the 2D fingerprint plot (Figure S3A), which constitute 15.5%. These hydrogen-bonded dimers are expanded into a 1D zigzag hydrogen-bonded chain connected by C12—H2B···S1 ($d_{(C12\cdots S1)} = 3.691$ Å) contacts running along the *c*-axis (Figure 3d). The second

TABLE 1 Crystal data and refinement parameters for Ni(II) dithiophosphonato complexes

Compound	$[Ni(L1)_2]$	$[Ni(L2)_2]$	$[Ni(L3)_2]$	$[Ni(L4)_2]$	$[Ni(L5)_2]$	$[Ni(L6)_2]$	$[Ni(L7)_2]$
Identification code	2054965	2054966	2104693	2054967	2018565	2097183	2061755
Empirical formula	$C_{18}H_{24}NiO_6P_2S_4$	$C_{20}H_{28}NiO_6P_2S_4$	$C_{22}H_{32}NiO_6P_2S_4$	$C_{24}H_{36}NiO_6P_2S_4$	$C_{26}H_{40}NiO_6P_2S_4$	$C_{26}H_{40}NiO_6P_2S_4$	$C_{30}H_{32}NiO_6P_2S_4$
Formula weight ($g.mol^{-1}$)	585.26	613.31	641.36	669.42	697.47	697.47	737.44
Temperature (K)	299	173	298	173	293	298	173
Radiation	MoKα (λ = 0.71073)	MoKα (λ = 0.71073)	MoKα (λ = 0.71073)	MoKα (λ = 0.71073)	MoKα (λ = 0.71073)	MoKα (λ = 0.71073)	MoKα (λ = 0.71073)
Crystal system	Monoclinic	Monoclinic	Orthorhombic	Triclinic	Triclinic	Monoclinic	Monoclinic
Space group	$P2_1/c$	$P2_1/c$	*Pbca*	*P*-1	*P*-1	$P2_1/c$	$P2_1/n$
a(Å)	16.3817(11)	8.9418(14)	13.6507(8)	7.6989(15)	8.3887(7)	19.9615(13)	13.8324(11)
b(Å)	8.5996(6)	17.118(3)	9.7558(6)	9.3652(18)	14.1029(10)	8.4109(6)	7.9441(6)
c(Å)	18.0039(13)	8.8754(14)	22.1172(13)	11.490(2)	15.0466(11)	22.1262(15)	14.9078(11)
α(°)	90	90	90	106.398(2)	66.894(2)	90	90
β(°)	8.5996(6)	94.757(3)	90	106.975(2)	84.304(3)	116.2830(10)	96.3780(10)
γ(°)	90	90	90	99.988(2)	86.506(3)	90	90
Crystal size (mm)	0.23 × 0.13 × 0.12	0.23 × 0.14 × 0.12	0.34 × 0.14 × 0.13	0.46 × 0.18 × 0.01	0.11 × 0.1 × 0.07	0.30 × 0.22 × 0.12	0.14 × 0.08 × 0.06
V ($Å^3$)	2525.0(3)	1353.8(4)	2945.4(3)	729.9(2)	1628.7(2)	3330.8(4)	1628.0(2)
Z	4	2	4	1	2	4	2
ρ_{calcd} ($g.\ cm^{-3}$)	1.540	1.505	1.446	1.523	1.422	1.391	1.504
μ (mm^{-1})	1.257	1.176	1.085	1.098	0.987	0.965	0.992
F(000)	1,208	636	1,336	350	732	1464	764
2θ range for data collection (°)	4.546–50.17	4.572–50.046	4.74–49.992	4.976–54.972	5.742–49.996	3.71–49.994	3.812–52.766
Index ranges	$-19 \le h \le 19$, $-10 \le k \le 10$, $-21 \le l \le 21$	$-10 \le h \le 10$, $-20 \le k \le 20$, $-8 \le l \le 10$	$-16 \le h \le 16$, $-11 \le k \le 11$, $-26 \le l \le 26$	$-9 \le h \le 9$, $-12 \le k \le 12$, $-14 \le l \le 14$	$-9 \le h \le 9$, $-16 \le k \le 16$, $-17 \le l \le 17$	$-23 \le h \le 20$, $-10 \le k \le 10$, $-26 \le l \le 26$	$17 \le h \le 17$, $-9 \le k \le 9$, $-18 \le l \le 18$
Reflections collected	31,577	5290	25,794	10,236	44,258	30,995	22,265

TABLE 1 (Continued)

Compound	$[Ni(L1)_2]$	$[Ni(L2)_2]$	$[Ni(L3)_2]$	$[Ni(L4)_2]$	$[Ni(L5)_2]$	$[Ni(L6)_2]$	$[Ni(L7)_2]$
Independent reflections	4489 [R_{int} = 0.0806, R_{sigma} = 0.0551]	2352 [R_{int} = 0.0237, R_{sigma} = 0.0323]	2586 [R_{int} = 0.0316, R_{sigma} = 0.0177]	3316 [R_{int} = 0.0352, R_{sigma} = 0.0365]	5663 [R_{int} = 0.0372, R_{sigma} = 0.0236]	5846 [R_{int} = 0.0405, R_{sigma} = 0.0312]	3322 [R_{int} = 0.0277, R_{sigma} = 0.0172]
Data/restraints/parameters	4489/0/286	2352/0/154	2586/41/192	3316/0/172	5663/0/361	5846/122/432	3322/0/198
Goodness-of-fit on F^2 (S)	1.015	1.081	1.081	1.047	1.208	1.064	1.054
Final R indexes [I > = 2σ (I)]	R_1 = 0.0434, wR_2 = 0.0899	R_1 = 0.0290, wR_2 = 0.0723	R_1 = 0.0386, wR_2 = 0.1032	R_1 = 0.0272, wR_2 = 0.0736	R_1 = 0.0620, wR_2 = 0.1255	R_1 = 0.0477, wR_2 = 0.1176	R_1 = 0.0233, wR_2 = 0.0604
Final R indexes (all data)	R_1 = 0.0825, wR_2 = 0.1051	R_1 = 0.0342, wR_2 = 0.0751	R_1 = 0.0468, wR_2 = 0.1094	R_1 = 0.0304, wR_2 = 0.0758	R_1 = 0.0735, wR_2 = 0.1299	R_1 = 0.0707, wR_2 = 0.1277	R_1 = 0.0279, wR_2 = 0.0634
Largest diff. peak and hole ($e.Å^{-3}$)	0.37/−0.27	0.38/−0.21	0.41/−0.28	0.50/−0.36	0.72/−0.67	0.34/−0.32	0.34/−0.19

most predominant contribution to the total HS by 19.0% is from the S···H/H···S interactions appearing as distinct spikes in the 2D fingerprint plot. Interestingly, as shown in Figure 3e, the C8—H8A···π_{phenyl} ($d_{(H\cdots\pi)}$ = 2.65 Å, Figure S2A) interaction contributed to stabilization of the 3D supramolecular network to form a honeycomb-like motif viewed down the *a*-axis. The closest C—H···π_{phenyl} interaction is seen in $[Ni(L1)_2]$, as illustrated in the shape index-mapped HS (Figure S2B).

In $[Ni(L2)_2]$, the weak C—H···O (C7—H7A···O1, $d_{(C7\cdots O1)}$ = 3.546 Å and C9—H9A···O2, $d_{(C9\cdots O2)}$ = 3.117 Å) and C—H···S (C3—H3···S1, $d_{(C3\cdots S1)}$ = 3.692 Å and C9—H9B···S2, $d_{(C9\cdots S2)}$ = 3.925 Å) hydrogen bonding interactions form a 2D supramolecular layers (Figure 4b–d). The 2D fingerprint regions of $[Ni(L2)_2]$ show that the S···H/H···S and O···H/H···O interactions constitute the significant area of the HS with the ratio of 22.7% and 16.5% (see Figure S5A). Moreover, these 2D layers are expanded into a 3D supramolecular network (Figure 4e) by the C8—H8A···π_{phenyl} ($d_{(H\cdots\pi)}$ = 2.72 Å, Figure S4A) interactions, as indicated in the shape index-mapped HS (Figure S4B).

As illustrated in Figure S4, the C···H/H···C interactions comprise 16.8% of the HS, which represent C—H···π interactions. In $[Ni(L3)_2]$, the C3—H3···O3 (d (C3···O3) = 3.645 Å, Figure 5c) hydrogen bonding interactions, which comprise the ratio of 12.4% of the HS (Figure SM7A), sustained by running along the *bc*-plane to form a 2D hydrogen-bonded layers (Figure 5b), which are stabilized by the short C—H···π contacts (C10—H10B···π, ($d_{(H\cdots\pi)}$ = 3.645(12) Å). Furthermore, the other C–H···π interactions (C9-H10C···π, ($d_{(H\cdots\pi)}$ = 3.636(4) Å) play a crucial role in the formation of the herringbone-like 3D supramolecular network (Figure 5d). The C···H/H···C intermolecular interactions that represent C—H···π interactions (Figure S6A) comprise 15.7% of the total HS for $[Ni(L3)_2]$. The HS shape index of $[Ni(L3)_2]$ shows concave curvature, where C—H···π interactions occur (Figure S6B).

In $[Ni(L4)_2]$, the weak C—H···O (C11—H11A···O2, $d_{(C11\cdots O2)}$ = 3.572 Å, Figure 6b) hydrogen bonding interactions (Figure 6c), which comprise 14.1% of the HS (Figure S9A), generated a 1D hydrogen-bonded chains along the *c*-axis. These chains are further linked by the short C—H···C contacts (C3—H3···C12, $d_{(H3\cdots C12)}$ = 2.88 Å; C8—H8A···C2, $d_{(H8A\cdots C2)}$ = 2.84 Å; C12—H12B···C5, $d_{(C12B\cdots C5)}$ = 2.82 Å), which are less than corresponding sum of the van der Waals distances ($r_{vdw}(C) + r_{vdw}(H)$ = 2.90 Å), to form a 2D hydrogen-bonded layers (Figure 6d). Moreover, the adjacent layers are connected through the weak π···π interactions ($d_{(\pi\cdots\pi)}$ = 4.255 Å) between the phenyl rings (Figure S8A) to form a 3D supramolecular network

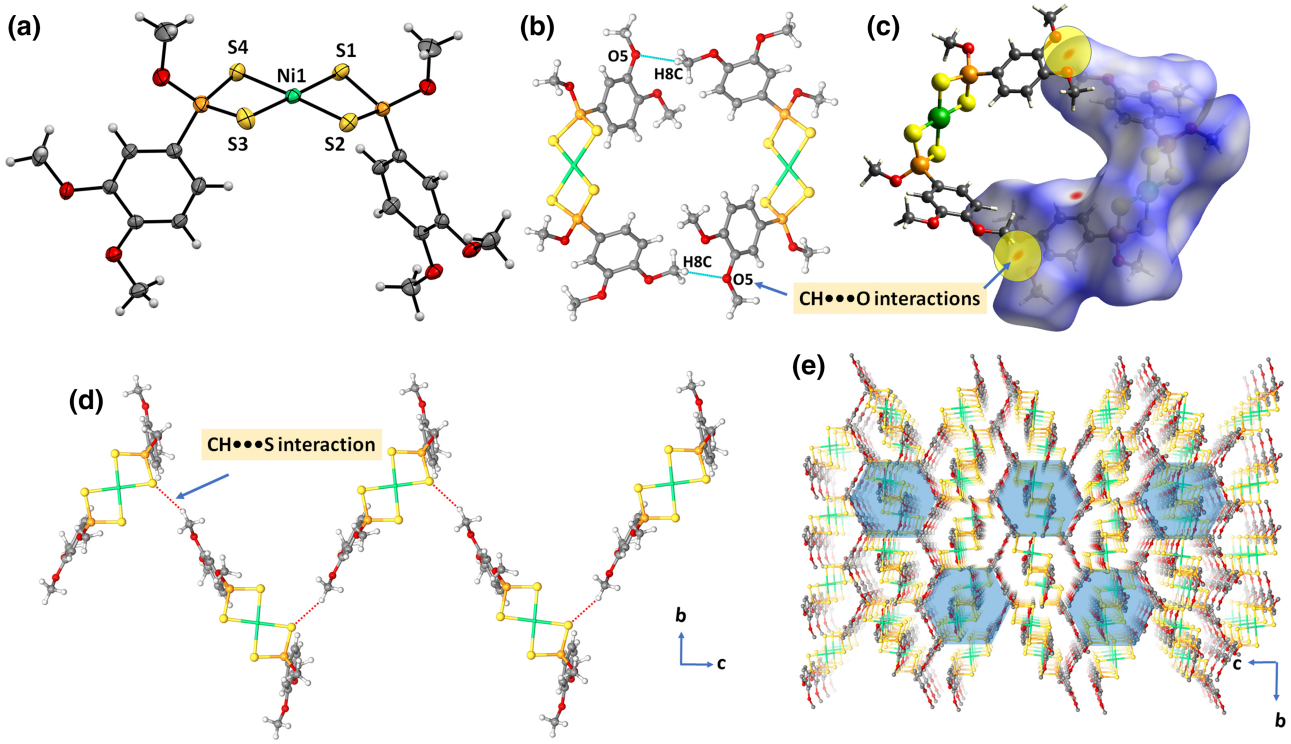

FIGURE 3 (a) Crystal structure of $[Ni(L1)_2]$ with displacement ellipsoids drawn at the 50% probability level. (b,c) Hirshfeld surface (HS) of $[Ni(L1)_2]$ mapped with d_{norm}, showing the C—H···O hydrogen bonding interactions. (d) View of the one-dimensional C—H···S hydrogen-bonded chains running along the crystallographic *c*-axis. (e) The illustration of the 3D supramolecular network showing the honeycomb-like motif

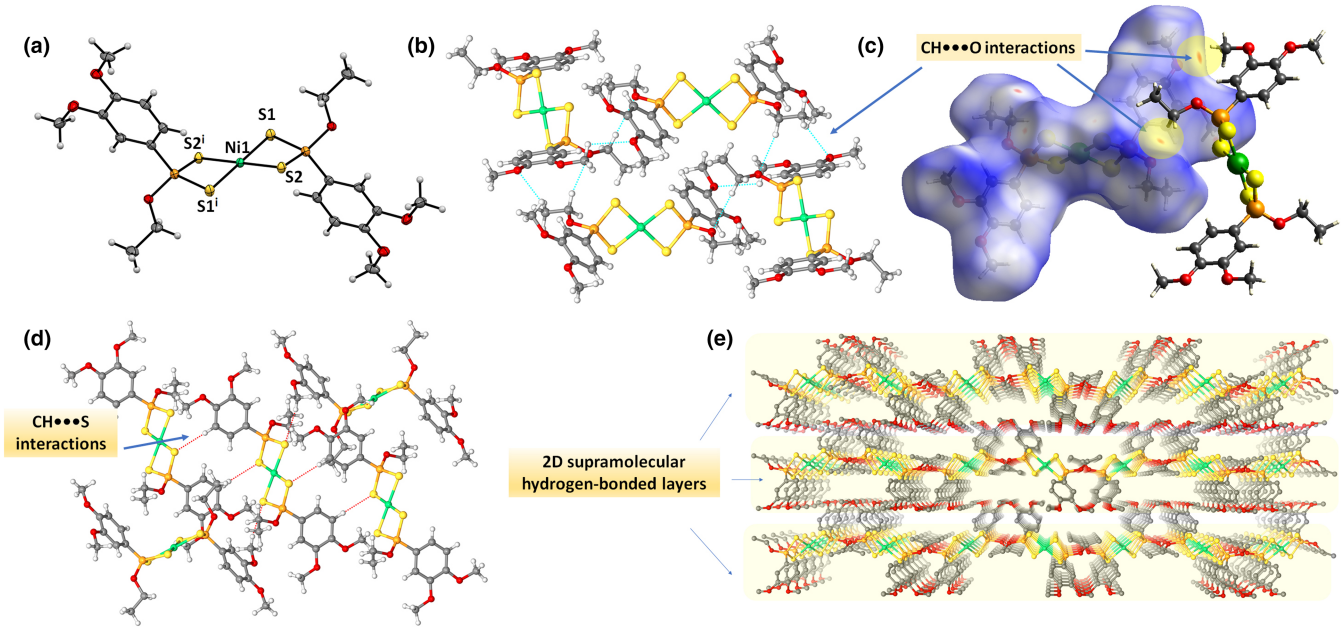

FIGURE 4 (a) Crystal structure of $[Ni(L2)_2]$ with displacement ellipsoids drawn at the 50% probability level (symmetry code: *i*: $-x+1$, $-y+1$, $-z$). (b,c) Hirshfeld surface (HS) of $[Ni(L2)_2]$ mapped with d_{norm}, showing the C—H···O hydrogen bonding interactions. (d) View of the C—H···S hydrogen bonding interactions in the crystal structure. (e) The illustration of the 3D supramolecular network showing 2D hydrogen-bonded layers

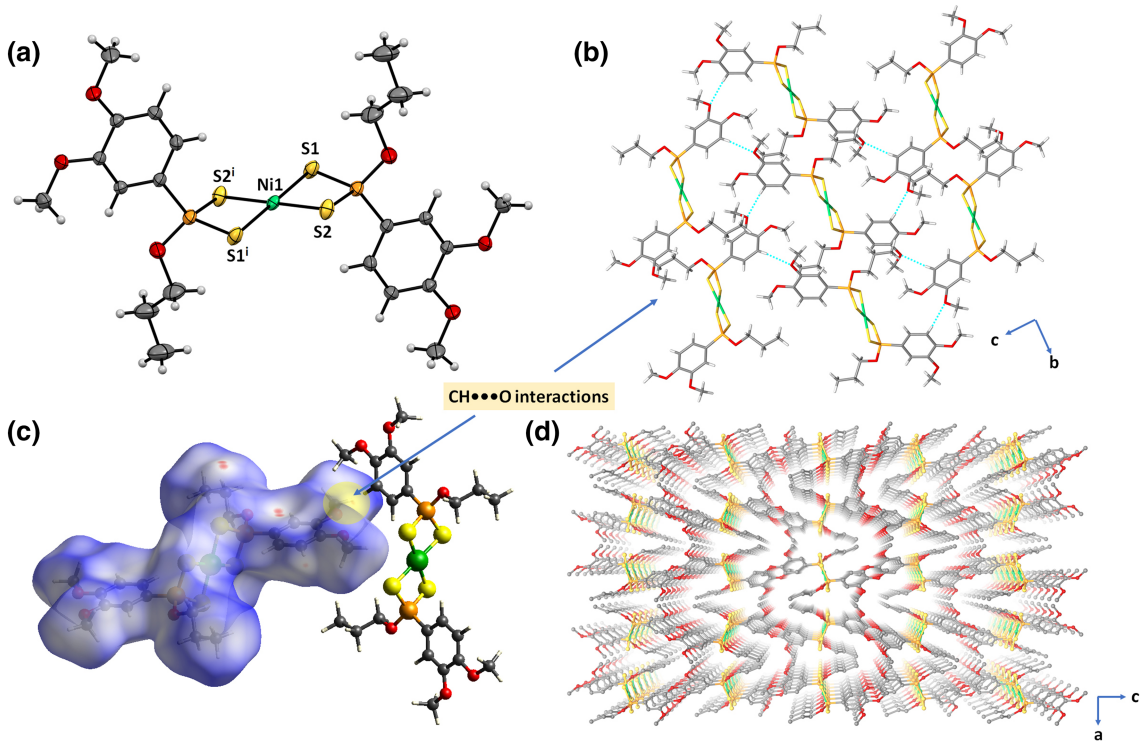

FIGURE 5 (a) Crystal structure of $[Ni(L3)_2]$ with displacement ellipsoids drawn at the 30% probability level (symmetry code: *i*: $-x+1$, $-y+1$, $-z$). (b,c) Hirshfeld surface (HS) of $[Ni(L3)_2]$ mapped with d_{norm}, showing the C—H···O hydrogen bonding interactions. (d) The illustration of the 3D supramolecular network showing the herringbone motif

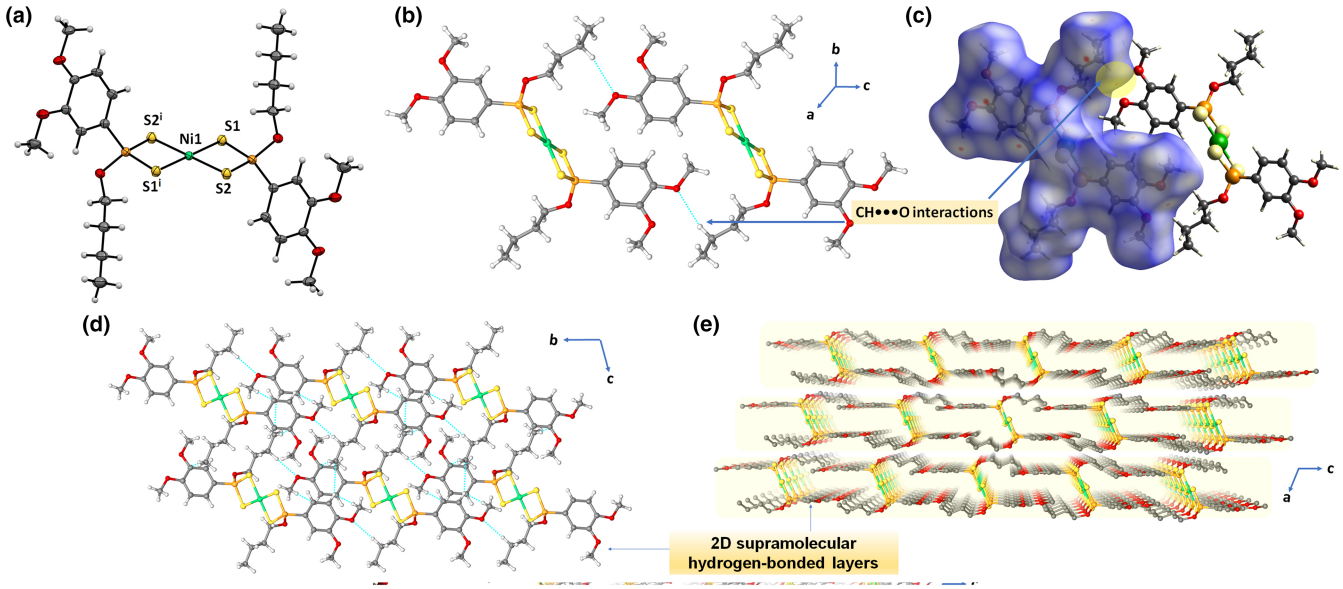

FIGURE 6 (a) Crystal structure of $[Ni(L4)_2]$ with displacement ellipsoids drawn at the 50% probability level (symmetry code: *i*: $-x+1$, $-y+2$, $-z+1$). (b,c) Hirshfeld surface (HS) of $[Ni(L4)_2]$ mapped with d_{norm}, showing the C—H···O hydrogen bonding interactions. (d) The 2D layers connected by the short C—H···O and C—H···C interactions. (e) Representation of 3D supramolecular network

(Figure 6e). This π···π interaction is observed by looking at the pattern of adjacent red and blue triangles on the HS shape index map (Figure S8B).

In $[Ni(L5)_2]$, the intermolecular C—H···O interactions (C12—H12A···O4, $d_{(C12\cdots O4)}$ = 3.634 Å; C12—H12A···O5, $d_{(C12\cdots O5)}$ = 3.285 Å; C9—H9B···O2,

$d_{(C9\cdots O2)}$ = 3.525 Å; C12—H12B···O3, $d_{(C12\cdots O3)}$ = 3.618 Å, Figure 7b) comprising 11.8% of the HS (Figure 7c, Figure S11A) form a 2D hydrogen-bonded layers along the *ac*-axis. In addition, the C—H···π interactions (C11—H11C···π, (d(H···π) = 2.73 Å, Figure S10A) contribute to the stabilization of the 3D supramolecular network (Figure 7d). The HS shape index of $Ni(L5)_2$] displays concave curvature, where C—H···π interactions occur (Figure S10B).

In $[Ni(L6)_2]$, two molecules in the asymmetric unit interact with each other through the weak intermolecular C—H···O interaction (C9—H9A···O4, $d_{(C9\cdots O4)}$ = 3.504 Å) and moderate π···π interaction ($d_{(\pi\cdots\pi)}$ = 3.838 Å) between the phenyl rings, as shown in Figures 8b and S12A. The HS shape index displays the evidence of the adjacent red and blue triangles on the shape index surface (Figure S12B). The other intermolecular C—H···O interaction (C18—H18B···O2, $d_{(C18\cdots O2)}$ = 3.504 Å) plays a key factor to construct the 3D herringbone-like supramolecular network (Figure 8d). As indicated Figure 8c, the weak C—H···O interactions make an 8.5% contribution to the total HS, (Figure S13A).

In $[Ni(L7)_2]$, the 3D supramolecular network is mainly stabilized by the weak C—H···O interaction (C11—H11···O3, $d_{(C11\cdots O3)}$ = 3.416 Å, Figure 9b) and the weak C—H···S interactions (C14—H14···S1, $d_{(C14\cdots S1)}$ = 3.857 Å; C6—H6···S2, $d_{(C6\cdots S2)}$ = 3.894 Å, Figure 9c,d). The C—H···O and C—H···S interactions comprise 14.1% and 12.9% of the total HS, respectively (Figure S15A). The C—H···π interactions (C13—H13···π, ($d_{(H\cdots\pi)}$ = 2.70 Å; C15—H15···π, ($d_{(H\cdots\pi)}$ = 2.95 Å, Figure S14A) also contributed the formation of a 3D network of crystal structure (Figure 9e). The C—H···π interactions in $[Ni(L7)_2]$ are easily can be seen in the HS shape index exhibiting concave curvature, where C—H···π interactions occur in Figure S14B.

To summarize the intermolecular interactions quantitatively, the 2D fingerprint plots exhibit that the most dominant interaction in $[Ni(Ln)_2]$ (n = 1–7) is the H/H interaction contributing to the total HS with the values equal to 41.1%, 42%, 47.5%, 51.5%, 56.7%, 59.4%, and 42.7%, respectively. This is probably due to the abundant aliphatic and aromatic hydrogen atoms in the compounds. The second most contributions to the total HS in $[Ni(L1\text{-}L6)_2]$ are from S/H···H/S interactions appearing as distinct spikes, which constitute 22.9%, 22.7%, 21.4%, 17.2%, 14.1, and 18%, respectively. This provides evidence for the important role of the C—H···S interactions in the stabilization of crystal structure. In the presence of benzyl, instead of aliphatic side groups, in $[Ni(L7)_2]$, the S/H···H/S interaction rate drops significantly. The fact that the side groups are aromatic makes C—H···π interactions be the second-highest contribution to the HS in $[Ni(L7)_2]$. The non-classical C—H···O hydrogen bonds are one of the other weak interactions observed in these

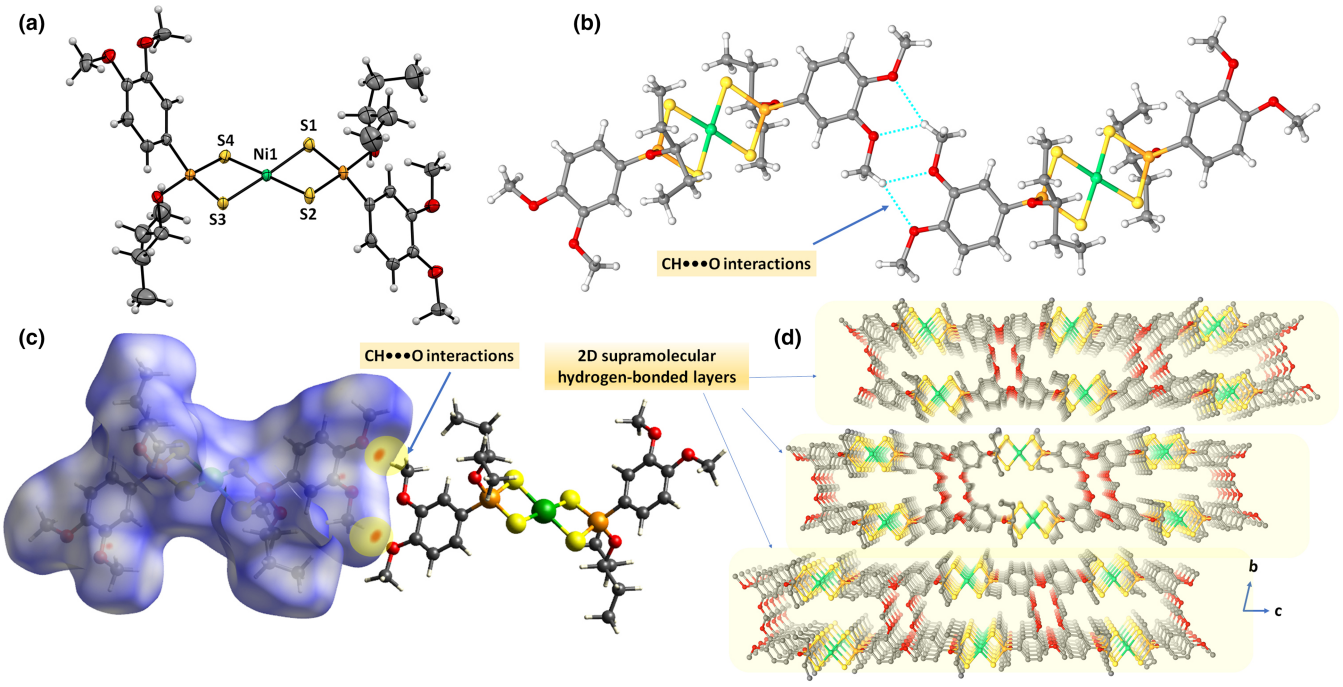

FIGURE 7 (a) Crystal structure of $[Ni(L5)_2]$ with displacement ellipsoids drawn at the 30% probability level (symmetry code: *i*: $-x+1$, $-y+1$, $-z$). (b,c) Hirshfeld surface (HS) of $[Ni(L5)_2]$ mapped with d_{norm}, showing the showing the C—H···O hydrogen bonding interactions. (d) Illustration of 3D supramolecular network

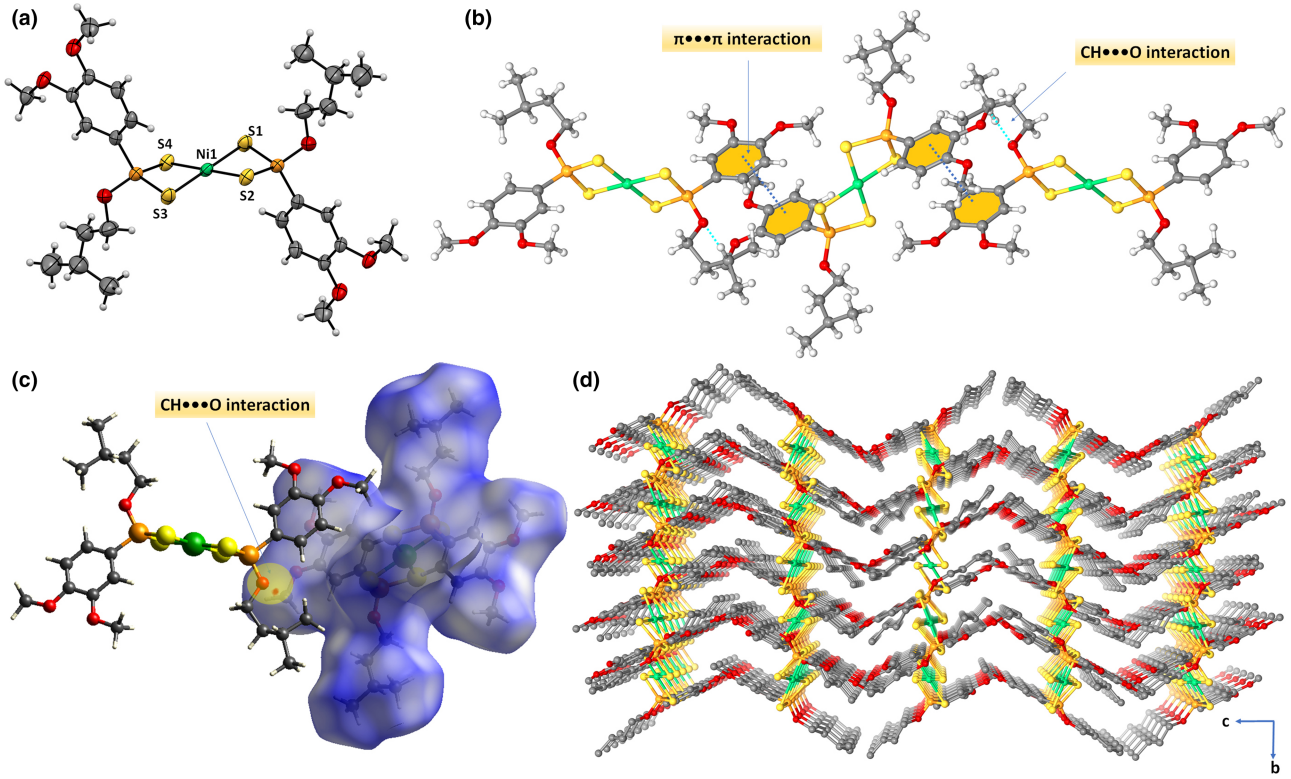

FIGURE 8 (a) Crystal structure of $[Ni(L6)_2]$ with displacement ellipsoids drawn at the 30% probability level (symmetry code: *i*: $-x+1$, $-y+1$, $-z$). (b) Perspective view of the C—H···O hydrogen bonding and the short π···π interaction. (c) Hirshfeld surface (HS) of $[Ni(L6)_2]$ mapped with d_{norm}, showing the C—H···O hydrogen bonding interactions. (d) The view of the 3D supramolecular network showing the herringbone motif

complex structures. It can be concluded that, as a general trend, the S/H···H/S interactions are the most important interactions after C—H···S interactions, comprising 15.5%, 16.5%, 12.4%, 14.1%, 11.8%, 8.5%, and 14.1% of the total HS, respectively. It is also worth noting that the C—H···π interactions in $[Ni(Ln)_2]$ ($n = 1$–7) make a remarkable contribution in the formation of supramolecular network with the ratio of 10.7%, 16.8%, 15.7%, 11.7%, 11.7%, 6.9%, and 25.4%, respectively. The shortest π···π interaction among all Ni(II) complexes was observed in the $[Ni(L6)_2]$, as exhibited large flat region on the curvedness mapped on the HS (Figure S13C).

3.3 | Optimized molecular structures of the complexes

The optimized 3D structural parameters of the complexes investigated were calculated using B3LYP/LANL2DZ/6-31+G(d,p) level in the ground state. The optimized molecular figures of the compounds are depicted in Figure 10a. Experimental and theoretical values of selected bond lengths and angles were listed in Table S7.

3.3.1 | Frontier orbitals and chemical parameters of the complexes

Frontier orbitals (HOMOs and LUMOs) are related to electron affinity and ionization potential (IP). These orbitals are very important for chemical reactivity. If the energy values of frontier orbitals are calculated, the chemical parameters such as the IP, the electron affinity (EA), the chemical hardness (η), the absolute electronegativity (χ), and the absolute softness (σ) of the molecules can be calculated by using to the Koopmans theorem.[76]

The chemical parameters and the energy gaps between HOMOs and LUMOs of the Ni(II) dithiophosphonato complexes were calculated by the DFT in the ground state. The total energies, calculated chemical parameters, and the energy gaps $\Delta E_{Gap} = (E_{LUMO} - E_{HOMO})$ were given in Table S9. As can be seen in the Table S9, the values of ΔE_{Gap} are 3.3641, 3.3625, 3.3590, 3.3598, 3.3758, 3.3644, and 3.3582 eV for the gas phases of the compounds $[Ni(Ln)_2]$ ($n = 1$–7), respectively. The configurations of HOMO and LUMO with energy levels are depicted in Figure 10b. In all the compounds, HOMOs are mainly localized on the whole molecule except for R_n groups, whereas LUMOs

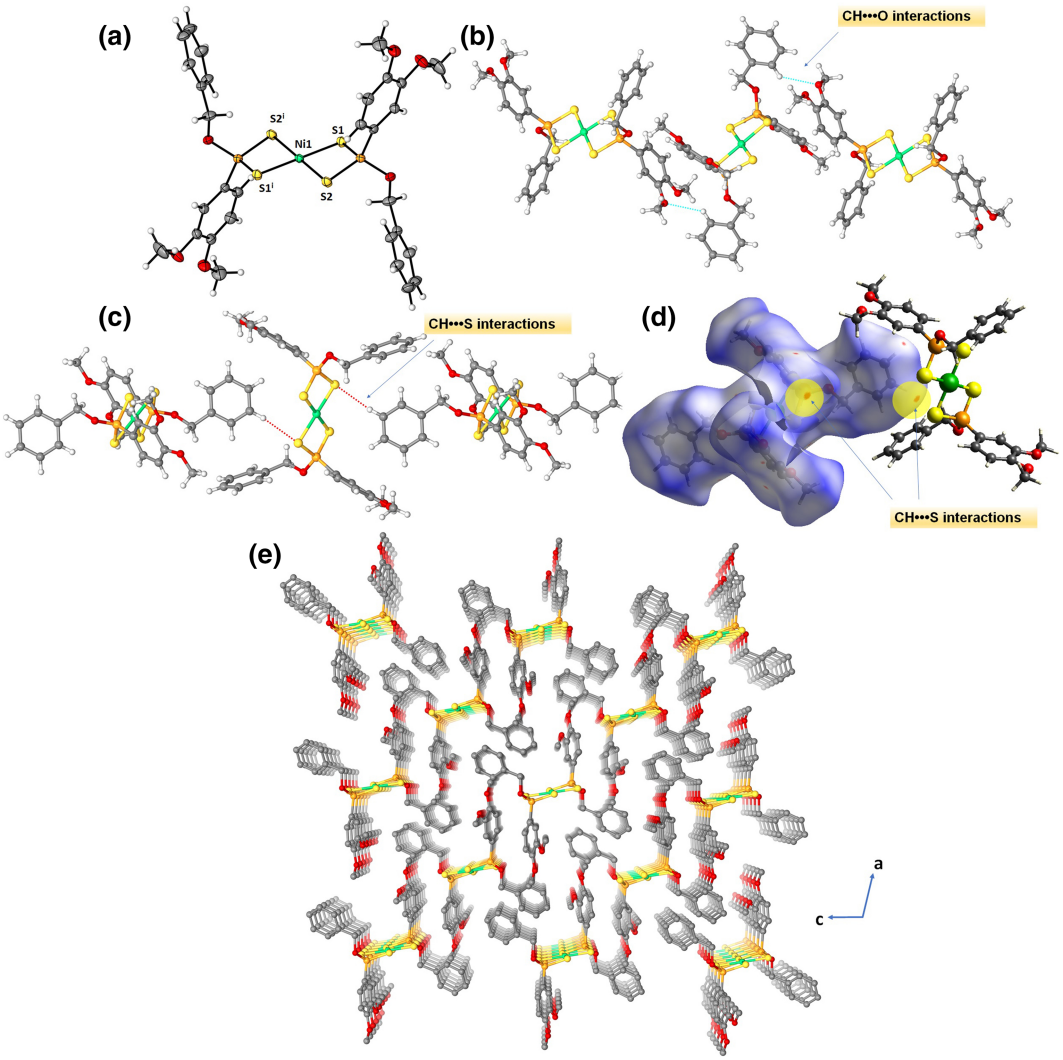

FIGURE 9 (a) Crystal structure of $[Ni(L7)_2]$ with displacement ellipsoids drawn at the 50% probability level (symmetry code: *i*: $-x+1$, $-y+2$, $-z+1$). (b,c) Perspective view of the C—H···O and C—H···S hydrogen bonding interactions. (d) Hirshfeld surface (HS) of $[Ni(L7)_2]$ mapped with d_{norm}, showing the C—H···S hydrogen bonding interactions. (e) View of the 3D supramolecular network

are mainly localized on PS_2 moiety and nickel atoms (Figure 10b).

3.3.2 | The MEP surfaces of the complexes

Electrostatic potential maps (MEPs) are valuable tools to describe the charge-related properties of molecules. They allow us to visualize the size and shape of molecules. The non-covalent interactions predicted by MEPs can allow us to predict the molecule's charge transfer and bioactivity centers. Conventionally, the negative regions are colored as red, whereas the positive regions are colored as blue in the MEPs. The negative regions exhibit higher electron density (electrophilic reactivity), whereas the positive regions exhibit low electron density (nucleophilic reactivity) in the MEPs. The MEP surfaces of the complexes were determined and visualized by the Gaussian 09 and Gauss-view visualization programs. MEPs were illustrated in Figure S16.

The oxygen atoms O3 (O4 for $[Ni(L1)_2]$ and $[Ni(L5)_2]$) of 3,4-dimethoxyphenyl groups in the compounds, the MEP diagrams indicated that the maximum electron densities (electrophilic reactivities) are 0.066, 0.067, 0.068, 0.067, 0.067, 0.067, and 0.068 a.u., respectively (Figure S16). The nucleophilic sites are illustrated in the MEP diagrams, Figure S16. These regions give preliminary information to predict possible intermolecular interactions.

3.3.3 | MDSs of the complexes

The MDS can be used to model the interactions between molecules and a target protein at the atomic level. These

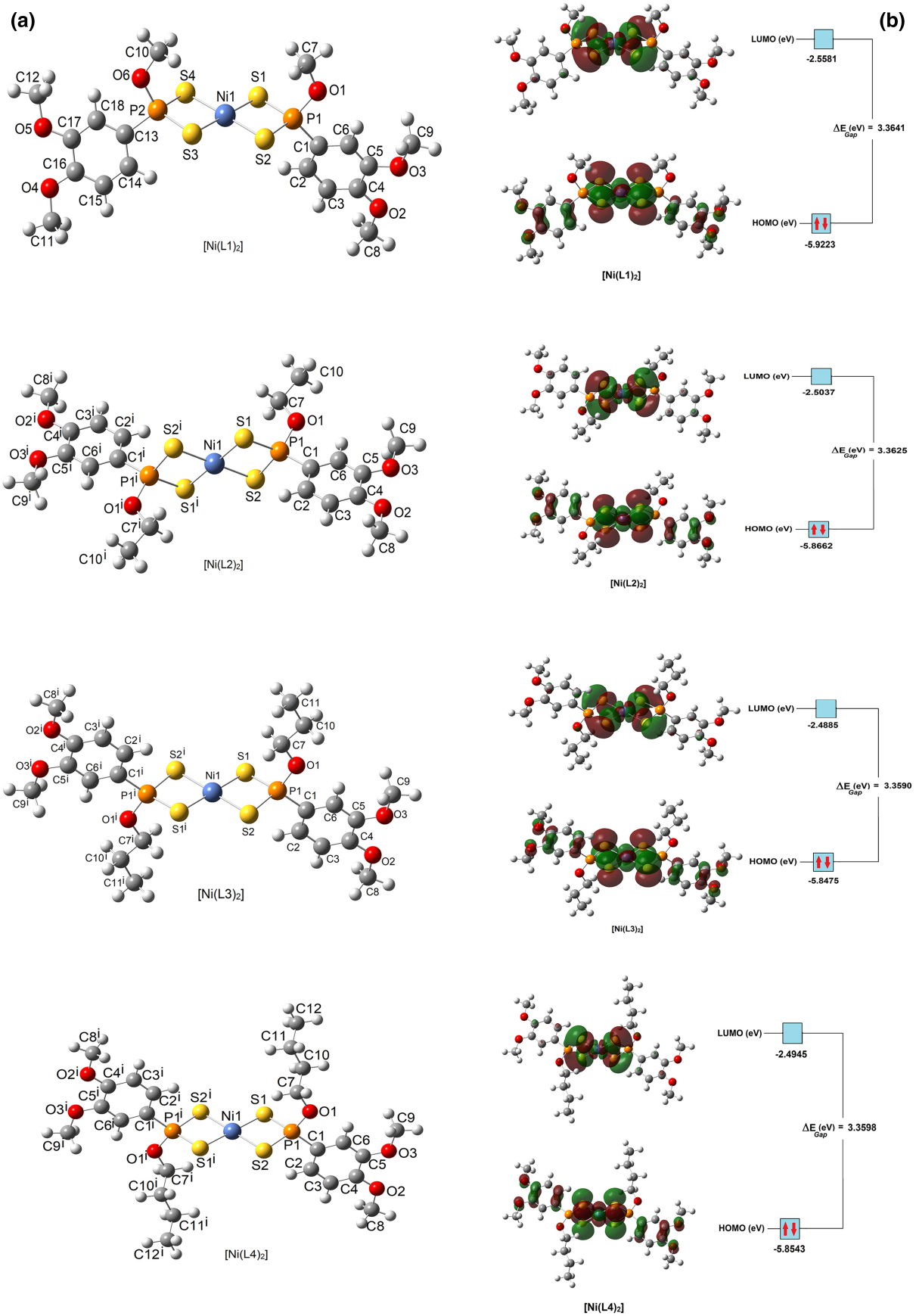

FIGURE 10 The optimized structures (a) highest occupied molecular orbital (HOMO) and lowest unoccupied molecular orbital (LUMO) surfaces electron density and band gap values (eV) (b) of the Ni(II) complexes

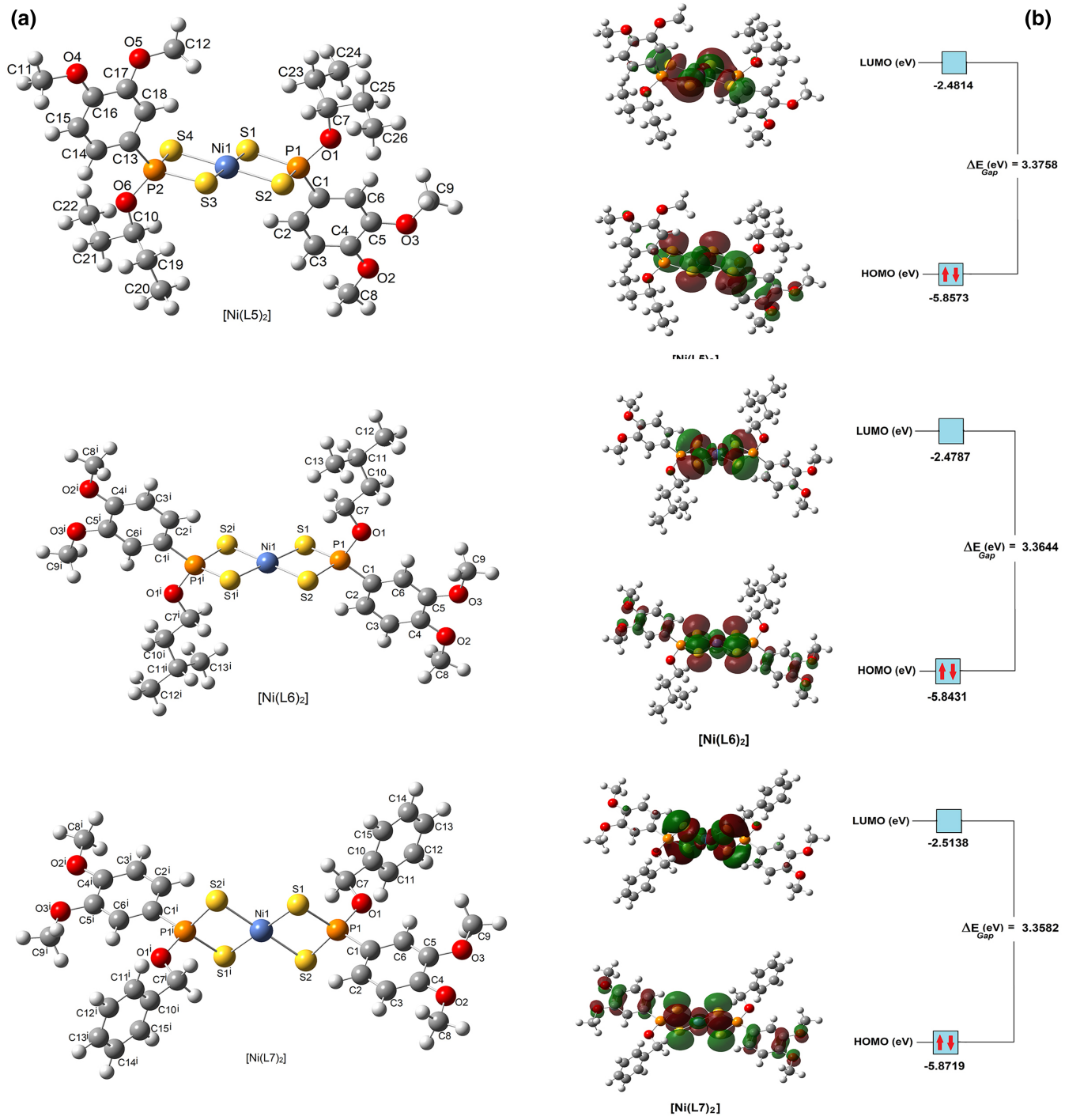

FIGURE 10 (Continued)

models serve in drug discovery and development studies and save time, thereby providing low costs. In this study, we first tested the Ni(II) complexes at various concentrations against cancer cell lines including HepG2 and DLD-1. As a second step, we predicted the potential interactions of $[Ni(Ln)_2]$ ($n = 1$–7) with proteins and compared the results with the corresponding experimental findings. The MDSs of the Ni(II) complexes were done with liver cancer protein, PDB ID: 3WZE and colon cancer antigen proteins, ID 2HQ6. The comparative bonding energies and RMSD values for each MDS are listed in Table S10. Energetically most favorable docked poses were obtained from the rigid molecular docking of each compound with 3WZE and 2HQ6 Figure 11a. The binding sites, binding types, and bond distances are given in Table S11. The 3D illustrations of the non-covalent

interactions between $[Ni(Ln)_2]$ ($n = 1$–7) and the proteins samples 3WZE and 2HQ6 were given in Figure 11b. For the docking interactions of $[Ni(Ln)_2]$ (n = 1–7) with PDB ID: 3WZE, the relative binding energy values are −6.5, −6.6, −6.5, −5.5, −5.5, −5.6, −5.9, and −8.2 kcal/mol, respectively. The corresponding values for docking studies with PDB ID: 2HQ6 are −5.8, −5.6, −5,5, −6.7, −7.2, −7.1, and −6.8 kcal/mol.

The complex $[Ni(L1)_2]$ binds at the active sites of amino acids, namely, ASP1046, ARG1027, PRO1068, ILE1025, ALA881, SER884, ARG1027, LEU889, and ILE888, of the liver cancer protein (PDB ID: 3WZE). The type of interactions is as follows: one the conventional hydrogen bonds, six carbon-involving hydrogen bonds, two (pi-system)-alkyl, one (pi-system)-sigma, and one (pi-system)-anion interactions. The conventional hydrogen bond length is 2.994 Å (between an OD2 oxygen on ASP1046 and S2 atom of dithiophosphonate-complex). On the other hand, six particular amino acids ASN103, GLN64, SER73, GLN112, ALA102, and HIS127 of colon cancer antigen proteins (PDB ID: 2HQ6) have been estimated to interact with $[Ni(L1)_2]$. The non-covalent interactions are as follows: three conventional hydrogen bonds; two carbon-involving hydrogen bonds; one (pi-system)-donor-metal acceptor bond; and one (pi-system)-donor-sulfur bond. The conventional hydrogen bond lengths are 3.157 Å (between NE2 nitrogen on GLN64 and O6 atom of OCH_3 group of dithiophosphonate-complex), 3.781 Å (between an O atom on ASN103 and S2 atom of dithiophosphonate-complex), and 3.384 Å (between an O atom on ASN103 and S3 atom of dithiophosphonate-complex).

The complex $[Ni(L2)_2]$ appears to be bound to the active sites of the amino acids HIS1026, LEU889, LEU1019, CYS1045, ASP1046, GLU885, ASP1046, and ARG1027 in the liver cancer protein (PDB ID: 3WZE) by two conventional hydrogen bonds; two (pi-system)-alkyl interactions; one alkyl-alkyl van der Waals bonds; three carbon-involving hydrogen bonds; one (pi-system)-anion interaction; and two (pi-system)-cation interactions. The conventional hydrogen bond lengths are 3.100 Å between HIS1026:O and S1 atom of

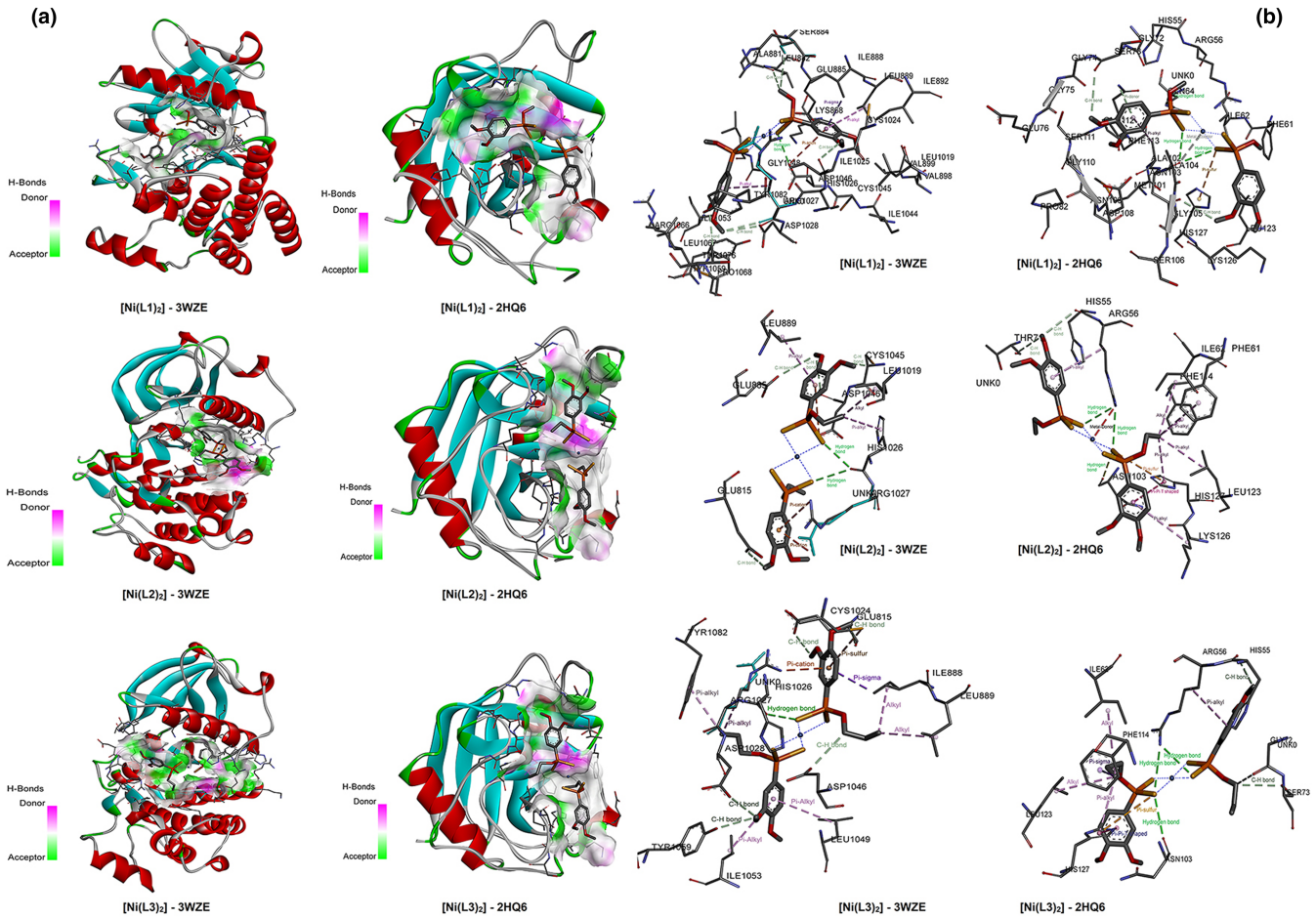

FIGURE 11 Energetically most favorable docked poses obtained from the rigid molecular docking of each complex with 3WZE and 2HQ6 (a) and the non-covalent interactions of the Ni(II) complexes (b)

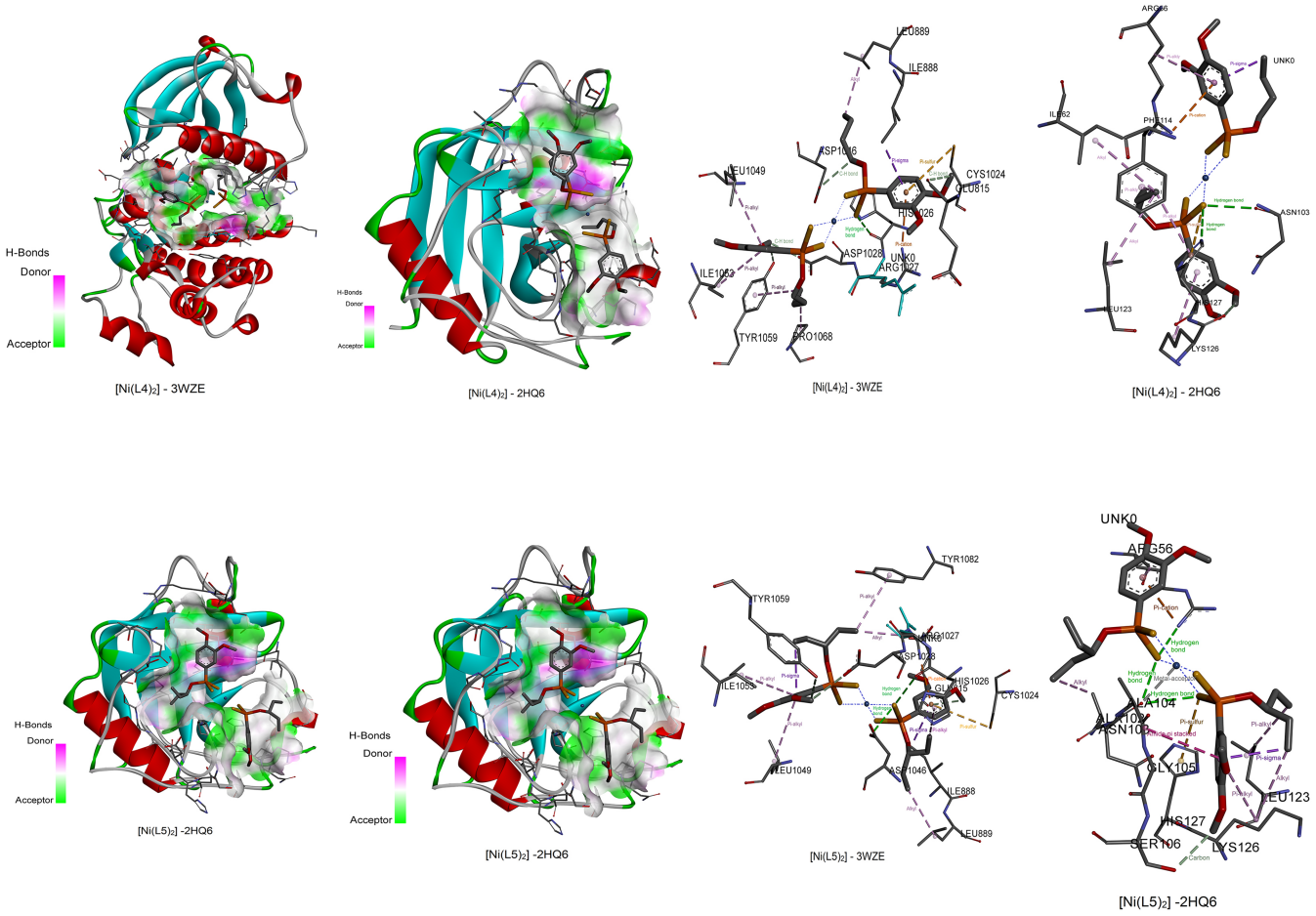

FIGURE 11 (Continued)

dithiophosphonato-complex and 3.527 Å between HIS1026:O and S2i atom of dithiophosphonate-complex. The complex binds at the active site of ARG56, ASN103, HIS127, LEU123, ILE62, PHE114, PHE61, LYS126, HIS55, and THR71 of the colon cancer antigen proteins (PDB ID: 2HQ6) by three conventional hydrogen bonds; one unfavorable metal-donor interaction; one T-shaped (pi-system)-(pi-system) interaction; six (pi-system)-alkyl interactions; two inter alkyl interactions, one (pi-system)-sulfur bond; and two carbon-involving hydrogen bond interactions. For the docking of colon cancer antigen proteins (PDB ID: 2HQ6) with $[Ni(L2)_2]$, the conventional hydrogen bond lengths are 3.482 Å between ARG56:NH1 and the atom S1 on the dithiophosphonato-complex; 3.686 Å between ARG56:NH1 and the atom S2i on the dithiophosphonate-complex; and 3.205 Å between an O atom on ASN103 and the S1 atom of the dithiophosphonato-complex.

The molecular docking results indicate that 14 amino acids, namely, HIS1026, LEU1049, ILE1053, TYR1082, ARG1027, LEU889, ILE888, TYR1059, ASP1028, ASP1046, GLU815, ARG1027, CYS1024, and ILE888 of the liver cancer protein (PDB ID: 3WZE), are found to interact with $[Ni(L3)_2]$ complex. The predicted 14 non-covalent interactions are of the types: one conventional hydrogen bond, three (pi-system)-alkyl interactions, three alkyl-alkyl van der Waals bonds, four carbon-involving hydrogen bonds, and three more interactions between (pi-system)-central cation, (pi-system)-sulfur, and (pi-system)-sigma bond. The conventional hydrogen bond length is 3.018 Å between HIS1026:O and the atom S2 of the dithiophosphonate-complex. On the other hand, eight particular amino acids ARG56, HIS127, LEU123, ILE62, PHE114, HIS55, GLY72, and SER73 of colon cancer antigen proteins (PDB ID: 2HQ6) have been estimated to interact with $[Ni(L3)_2]$. The 11 non-covalent interactions are as follows: three conventional hydrogen bonds; two (pi-system)-alkyl and two alkyl-alkyl interactions; two carbon-involving hydrogen bonds; and three more interactions between (pi system)-sulfur, (pi-system)-sigma bond, and one T-shaped (pi-system)-(pi-system) interactions. The conventional hydrogen bond lengths are 3.507 Å (between the NH1 nitrogen atom on ARG56 and one of the S atoms on

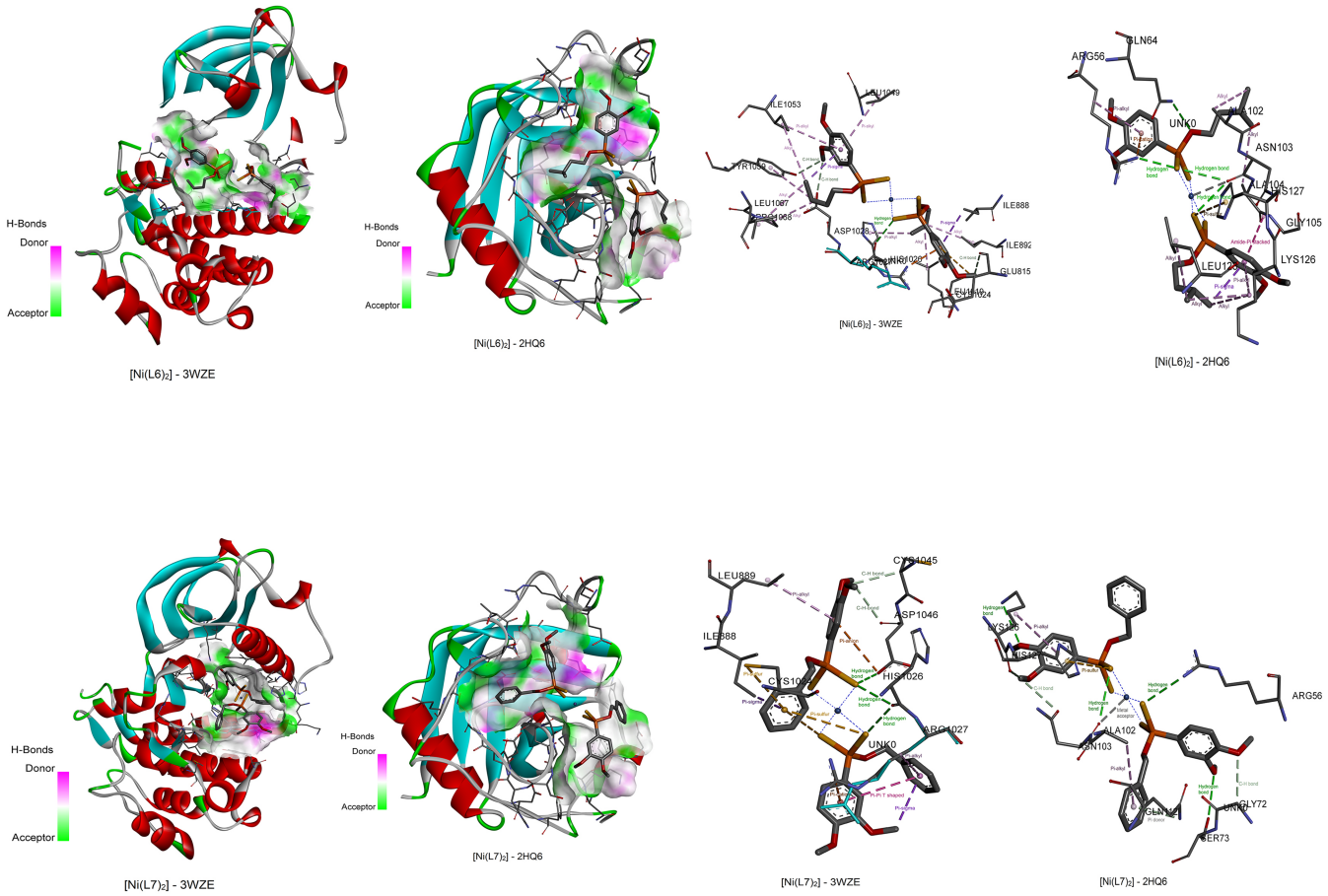

FIGURE 11 (Continued)

dithiophosphonato-complex); 3.681 Å (between the NH1 nitrogen atom of ARG56 and another S atom on dithiophosphonato-complex); and 3.303 Å (between an O atom on ASN103 and S atom of dithiophosphonato-complex.

The complex $[Ni(L4)_2]$ binds at the active sites of HIS1026, PRO1068, LEU889, TYR1059, LEU1049, ILE1053, TYR1059, ASP1028, ASP1046, ILE888, ARG1027, and CYS1024 of the liver cancer protein (PDB ID: 3WZE). The type of interactions is as follows: one conventional hydrogen bond; two alkyl-alkyl and two (pi-system)-alkyl interactions; three carbon-involving hydrogen bonds; and three more interactions between (pi-system)-sigma bond, (pi-system)-cation, and (pi-system)-sulfur. The conventional hydrogen bond length is 3.506 Å (between an O atom on HIS1026 and the S1 atom of dithiophosphonato-complex). The molecular docking results between $[Ni(L4)_2]$ and the colon cancer antigen proteins (PDB ID: 2HQ6) show that the complex binds to active sites on ASN103, HIS127, ILE62, LEU123, HIS127, PHE114, LYS126, and ARG56 of 2HQ6. The non-covalent interactions are as follows: two conventional hydrogen bonds; four (pi-system)-alkyl and two alkyl-alkyl interactions and two more interactions between (pi-system)-sulfur and (pi-system)-cation. The conventional hydrogen bond lengths are 3.163 Å (between an O atom on ASN103 and S1 atom of dithiophosphonate-complex) and 3.551 Å (between NE2 nitrogen on HIS127 and S1 atom of dithiophosphonato-complex).

The docking studies between $[Ni(L5)_2]$ and 3WZE indicate that the amino acids HIS1026, ASP1046, ARG1027, LEU889, TYR1082, ILE1053, LEU1049, CYS1024, TYR1059, and GLU815 interact with the complex. The non-covalent interactions between the complex and the liver cancer protein (PDB ID: 3WZE) are as follows: two conventional hydrogen bonds, four (pi-system)-alkyl interactions, two alkyl-alkyl interactions, one (pi-system)-sulfur, and one (pi-system)-cation interaction and two carbon involving-hydrogen bond interactions. There are the conventional hydrogen bonds are of the lengths, 3.232 Å (between an O atom on HIS1026 and an S atom on dithiophosphonato-complex) and 3.524 Å (between OD2 oxygen on ASP1046 and S atoms of dithiophosphonato-complex). Docking studies also show that six different amino acids ARG56, ASN103, LYS126, ALA102, LEU123, ALA104, and GLY105 of colon cancer

antigen proteins (PDB ID: 2HQ6) interact with the [Ni(L5)$_2$]. The non-covalent interactions are as follows: three conventional hydrogen bonds, two (pi-system)-alkyl, and three alkyl-alkyl interactions along with one amide-pi stacked interaction and one carbon-involving hydrogen bonds. The conventional hydrogen bond lengths are 3.276 Å (between NH1 nitrogen on ARG56 and S1 atom of dithiophosphonato-complex), 3.441 Å (between an O atom on ASN103 and S2i of dithiophosphonato-complex), and 3.355 Å (between an O atom on ASN103 and S1 atom of dithiophosphonato-complex).

The complex [Ni(L6)$_2$] binds at the active site of HIS1026, ASP1028, TYR1059, GLU815, PRO1068, LEU1067, ILE1053, LEU1049, LEU1019, ILE892, ILE888, and ARG1027 of the liver cancer protein (PDB ID: 3WZE) with one conventional hydrogen bond, one alkyl, eight (pi-system)-alkyl, three carbon involving-hydrogen bond, one for (pi-system)-sigma, and one (pi-system)-cation interactions. The conventional hydrogen bond length is 3.053 Å (between an O atom on HIS1026 and S1 atom of dithiophosphonato-complex). The molecular docking results between [Ni(L6)$_2$] with the colon cancer antigen proteins (PDB ID: 2HQ6) predict that the complex [Ni(L6)$_2$] binds at the active site of HIS1026, ASP1028, TYR1059, GLU815, PRO1068, LEU1067, ILE1053, LEU1049, LEU1019, ILE892, ILE888, and ARG1027 of 2HQ6. The non-covalent interactions are as follows: one conventional hydrogen bond, eight (pi-system)-alkyl, three carbon involving-hydrogen bond, and one (pi-system)-sigma and (pi-system)-cation interactions. The conventional hydrogen bond length is 3.053 Å between HIS1026:O and S1 atom of dithiophosphonato-complex.

The molecular docking results indicate that nine amino acids, namely, HIS1026, ARG1027, LEU889, ILE888, ARG1027, ASP1046, CYS1024, ASP1046, and CYS1045 of the liver cancer protein (PDB ID: 3WZE), are found to interact with [Ni(L7)$_2$] complex. The predicted non-covalent interactions are of the types: two conventional hydrogen bonds, two carbon involving-hydrogen bonds, two (pi-system)-alkyl, one (pi-system)-sigma, one (pi-system)-anion, and two (pi-system)-cation interactions. The conventional hydrogen bond lengths are 3.042 Å (between an O atom on HIS1026 and S1 atom of dithiophosphonato-complex) and 3.091 Å (between an O atom on HIS1026 and S2i atom of dithiophosphonato-complex). Finally, docking studies also show that nine different amino acids ARG56, LYS126, ASN103, SER73, LYS126, ALA102, GLN112, ASN103, and GLY72 of colon cancer antigen proteins (PDB ID: 2HQ6) interact with the [Ni(L7)$_2$]. The non-covalent interactions are as follows: four conventional hydrogen bonds, two carbon involving-hydrogen bonds, two (pi-system)-alkyl, one (pi-system)-donor hydrogen, and one metal acceptor interactions. The conventional hydrogen bond lengths are 3.591 Å between ARG56:NH1 and S1, 3.119 Å between LYS126:NZ and O3i atom of 3,4-dimethoxyphenyl, 3.718 Å between ASN103 and S2i atom of dithiophosphonato-complex, and 3.098 Å between GLY72:CA and O3 atom of 3,4-dimethoxyphenyl in the complex.

The lowering of the HOMO–LUMO energy gap value has a substantial influence on the intermolecular charge transfer. The low HOMO–LUMO energy gap always refers to lower kinetic stability and higher chemical reactivity. As for the DFT results, the energy gap ΔE_{Gap} (eV) of the complex [Ni(L7)$_2$] is lower than the other Ni complexes used in this study (Table S9**)**. The energy gap ΔE_{Gap} (eV) of the complex [Ni(L7)$_2$] is especially noteworthy to predict potential non-covalent interactions with colon cancer antigen proteins (PDB ID: 2HQ6). Consequently, according to all of the molecular docking results, we can say that the bioactivity of the investigated complexes with 2HQ6 (colon cancer antigen proteins) is higher than that between the investigated Ni complexes and 3WZE (the liver cancer protein).

The molecular and crystal structures of the complexes in the study were determined using single-crystal X-ray structure analyses. The optimized geometries from X-ray structure analyses were used for MDS of the complexes. The MDS studies of the Ni(II) complexes on the liver cancer protein, PDB ID: 3WZE and colon cancer antigen proteins, ID 2HQ6 were investigated to predict potential interactions. The small HOMO–LUMO energy gap value has a significant effect on intermolecular charge transfer. The low HOMO–LUMO energy gap always refers to lower kinetic stability and higher chemical reactivity. As can be seen in Table S9, the values of ΔE_{Gap} (eV) are 3.3641, 3.3625, 3.3590, 3.3598, 3.3758, 3.3644, and 3.3582 eV for the gas phases of the complexes [Ni(L1)$_2$], [Ni(L2)$_2$], [Ni(L3)$_2$], [Ni(L4)$_2$], [Ni(L5)$_2$], [Ni(L6)$_2$], and [Ni(L7)$_2$], respectively. These values are very close to each other. Therefore, it is not appropriate to compare the values of the energy gaps ΔE_{Gap} (eV) of the investigated complexes in order to explain the non-covalent interactions of the compounds with PDB ID: 3WZE and colon cancer antigen protein ID 2HQ6 for MDS. Except for [Ni(L4)$_2$] and [Ni(L7)$_2$] complexes, the others did not have a significant effect on the growth of liver cancer cells, while it was observed that none of the nickel complexes were effective on colon cancer under the same experimental conditions. The detailed experimental results and comparison have been given in In vitro cytotoxic activity studies. The comparative predicted binding sites, binding types, and bond distances for each the

MDS studies of the Ni(II) complexes on the liver cancer protein, PDB ID: 3WZE and colon cancer antigen proteins, PDB ID: 2HQ6 were listed in Table S10. The 3D illustrations of the predicted non-covalent interactions between $[Ni(Ln)_2]$ ($n = 1$–7) and the proteins samples 3WZE and 2HQ6 were also given in Figure 11b. According to MDS results, the bioactivities of the investigated complexes with colon cancer antigen proteins (PDB ID: 2HQ6) were higher than the bioactivities between the investigated complexes and liver cancer proteins (PDB ID: 3WZE).

3.4 | In vitro cytotoxic activity studies

The cytotoxic activities of compounds were tested at 5, 10, 20, 50, 100, and 200 μM concentrations in two human cancer cell lines, including HepG2 and DLD-1 for 48 h. The results are given in Table 2.

As can be seen in the results in Table 2, while the designed organic molecules were not effective in the HepG2 cell line, it was observed that two of the nickel complexes of these molecules were effective on cell growth. These two complexes having the codes of $[Ni(L4)_2]$ and $[Ni(L7)_2]$ had cytotoxic activity on HepG2 cell line with IC_{50} values of 181.1 and 173.2 μM, respectively. These $[Ni(L4)_2]$ and $[Ni(L7)_2]$ complexes, which contain *n*-butyl and benzyl groups in their structures, respectively, demonstrated more toxic effects on liver cells than on colon cancer cells. However, other compounds ($[NH_4Ln]$ ($n = 1$–7), $[Ni(L1)_2]$-$[Ni(L3)_2]$, $[Ni(L5)_2]$, $[Ni(L6)_2]$) except of these mentioned complexes ($[Ni(L4)_2]$ and $[Ni(L7)_2]$) did not have a significant effect on the growth of liver cancer cells and the calculated IC_{50} values were found to be greater than 200 μM.

Comparison of the data obtained within the set of synthesized compounds $[NH_4Ln]$ and $[Ni(Ln)_2]$ ($n = 1$–7) show that aliphatic side chains revealed a drastic change in the activities of these compounds. According to the structure–activity relationship (SAR) studies, a compound $[NH_4L5]$ containing 3-pentyl substituent on the phenyl ring demonstrated more antiproliferative activity compared with that of other synthesized new compounds $[NH_4L1]$-$[NH_4L4]$, $[NH_4L6]$, $[NH_4L7]$, and $[Ni(L1)_2]$-$[Ni(L7)_2]$ with IC_{50} value of 68.2 μM in DLD-1 cell line. Other active compounds towards the DLD-1 cell line were $[NH_4L2]$, $[NH_4L3]$, and $[NH_4L6]$ with IC_{50} values of 131.3, 151.2, and 118.0 μM, respectively. However, under the same experimental conditions, it was observed that none of the nickel complexes were effective on colon cancer, and the related cancer cells grew as in the negative control. In a nutshell, all tested molecules and their nickel complexes exhibited lower cytotoxic activity in both liver and colon cancer cell lines than that of conventional chemotherapeutic drug cisplatin.

The dose-dependent effects of new compounds on cell viability ratio are given in Figures 12 and 13.

As can be seen in Figures 12 and 13, the viability ratio of cells changed depending on concentrations tested of the compounds and cisplatin for two cell lines. For the majority of compounds tested in this study, the highest cell viability was seen at concentrations of 5, 10, 20, 50, and 100 μM. Cell viability ratios were calculated as 88.36%, 80.37%, 94.75%, 79.12%, 55.26%, 53.00%, 71.96%, 66.63%, 59.14%, 64.64%, 41.51%, 50.30%, 37.64%, and 37.23% in HepG2 cells at 200 μM concentration of compounds $[NH_4Ln]$ and $[Ni(Ln)_2]$ ($n = 1$–7), respectively. At 200 μM concentration of compounds $[NH_4Ln]$ and $[Ni(Ln)_2]$ ($n = 1$–7), the viability ratios were calculated as 62.10%, 52.49%, 57.26%, 64.54%, 48.57%, 52.17%, 64.58%, 95.82%, 98.56%, 96.61%, 69.36%, 53.20%, 48.92%, and 55.64% for DLD-1 cells, respectively.

It is seen in Figure 13 that the activity of ligands in colon cancer cells is higher than their nickel complexes. For example, while the cell viability ratio was obtained as 56.77% in 100 μM of $[NH_4L2]$, this ratio was

TABLE 2 IC_{50} results for compounds against cancer cell lines

	IC_{50} (μM)		IC_{50} (μM)		
Ligands	**HepG-2**	**DLD-1**	**HepG-2**	**DLD-1**	**Complexes**
$[NH_4L1]$	>200	>200	>200	>200	**$[Ni(L1)_2]$**
$[NH_4L2]$	>200	131.3	>200	>200	**$[Ni(L2)_2]$**
$[NH_4L3]$	>200	151.2	>200	>200	**$[Ni(L3)_2]$**
$[NH_4L4]$	>200	>200	181.1	>200	**$[Ni(L4)_2]$**
$[NH_4L5]$	>200	**68.2**	>200	>200	**$[Ni(L5)_2]$**
$[NH_4L6]$	>200	118.0	>200	>200	**$[Ni(L6)_2]$**
$[NH_4L7]$	>200	>200	173.2	>200	**$[Ni(L7)_2]$**
Cisplatin	53.4	56.1			

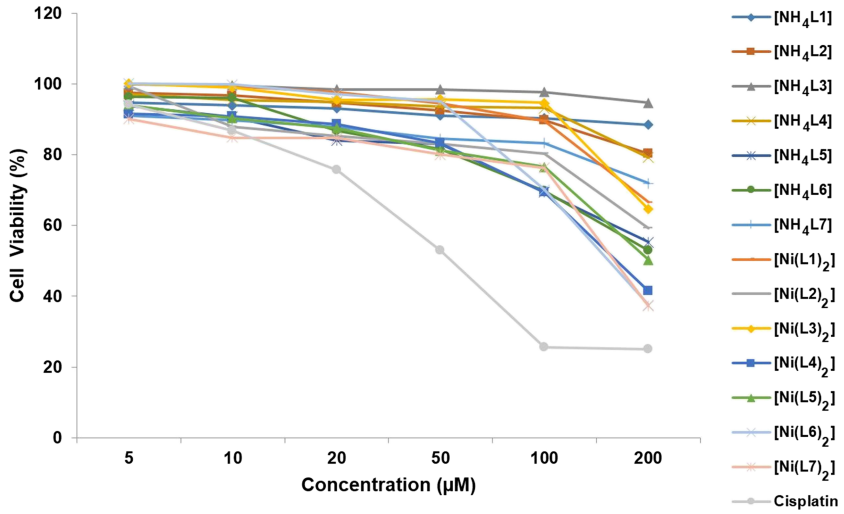

FIGURE 12 Dose-dependent antiproliferative effect of compounds and cisplatin on HepG2 cells for 48 h

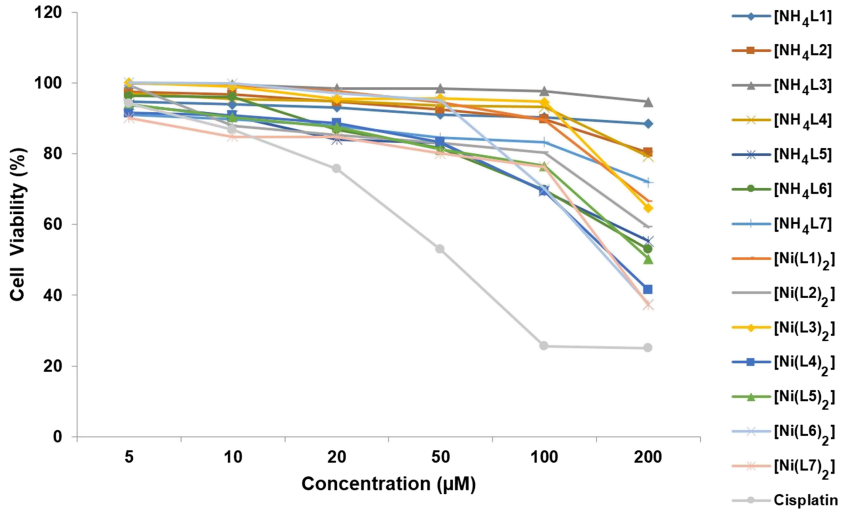

FIGURE 13 Dose-dependent antiproliferative effect of compounds and cisplatin on DLD-1 cells for 48 h

calculated as 100% when the complex of this compound was used.

4 | CONCLUSIONS

In an effort to create alternatives to the well-known perthiophosphonic acid anhydrides such as Lawesson reagent and Belleau reagents, we investigated on the new reagent, SAV-A1, with an emphasis on a less laborious procedure. This compound was used in the synthesis of structurally diverse organo-dithiophosphonic acid ammonium salts, and the anions of these salts were used in the preparation of new dithiophosphonato Ni(II) complexes. The structures of the ligands and the complexes were elucidated by spectroscopic techniques. The ^{13}C-NMR spectra of the aromatic parts of the compounds display interesting features.

The theoretically calculated structural parameters of the [Ni(Ln)$_2$] complexes were compared with the molecular structures obtained from X-ray analysis by using DFT. Total molecular energies, HOMO–LUMO band energy gaps, the chemical parameters, the HOMO and LUMO diagrams, and MEP analysis of the complexes were reported by the quantum mechanical calculations. Energetically, the most favorable poses during docking were also obtained from the rigid molecular docking of each Ni complex with liver cancer protein, PDB ID: 3WZE and colon cancer antigen proteins, ID 2HQ6. The binding sites, types of interaction, and bond distances are predicted by MDS of the compounds. According to the theoretical results, the HOMO–LUMO band energy gap ΔE_{Gap} (eV) of the complex [Ni(L7)$_2$] is lower than those of the others.

Molecular docking results show that the bioactivities of the investigated complexes with 2HQ6 (colon cancer

antigen proteins) are higher than that between the complexes and 3WZE (the liver cancer protein).

The compounds concerned were also tested against two different cell lines for evaluating the anti-cancer potentials. It was found that some of the compounds prepared have a toxic effect on the screened cell lines. In particular, the compound [NH_4L5] was found to be more cytotoxic effect with an IC_{50} value of 68.2 μM in DLD-1. The theoretical calculation results appear to agree well with the experimental findings. [Ni(L7)$_2$] was found to be the most effective complex, among metals against HepG2 cells.

ACKNOWLEDGMENTS

This study is supported by the Project Coordination Application and Research Center of Yozgat Bozok University (BAP 6602c-FEN/20-359). Single crystal X-ray studies of the [Ni(Ln)$_2$] complexes (n = 1, 2, 3, 4, 6, and 7) were supported by the Research Foundation of Marmara University, Commission of Scientific Research Project (BAPKO; Project No: FDK-FDK-2021-10339). It is also supported by Suleyman Demirel University Research Fund (TSG-2021-8458) for anticancer studies. The numerical calculations reported in this paper were fully/partially performed at The Scientific and Technological Research Council of Turkey (TUBITAK) ULAKBIM, High Performance and Grid Computing Center (TRUBA resources). The authors would like to thank Prof. Dr. Hamza Yılmaz for sharing his knowledge and experience. The authors would like to also thank the Genome and Stem Cell Center (Erciyes University, GENKOK, Kayseri/Turkey) for allowing them to do cell culture studies in their laboratory.

CONFLICT OF INTEREST

The authors declare that they have no known competing financial interests or personal relationships that could have influenced the work reported in this study.

AUTHOR CONTRIBUTIONS

Elif Bulat: Conceptualization; formal analysis; funding acquisition; investigation; methodology; visualization; writing–original draft. **Ertuğrul Gazi Sağlam:** Conceptualization; formal analysis; funding acquisition; investigation; resources; supervision; validation; visualization; writing–original draft; writing–review & editing. **Celal Tuğrul Zeyrek:** Formal analysis; investigation; resources; software; visualization; writing–original draft; **Senem Akkoç:** Investigation; validation; visualization; writing – original draft**; Yunus Zorlu:** Formal analysis; investigation; software; validation; visualization; writing–original draft; **Hakan Dal:** Funding acquisition; investigation; validation; visualization; writing–original draft.

ORCID

Elif Bulat https://orcid.org/0000-0002-2164-3641
Ertuğrul Gazi Sağlam https://orcid.org/0000-0002-7719-3934
Celal Tuğrul Zeyrek https://orcid.org/0000-0001-6744-7841
Senem Akkoç https://orcid.org/0000-0002-1260-9425
Yunus Zorlu https://orcid.org/0000-0003-2811-1872
Hakan Dal https://orcid.org/0000-0003-0518-522X

REFERENCES

[1] I. S. Nizamov, D. A. Terenzhev, G. G. Shumatbaev, I. D. Nizamov, D. R. Islamov, O. V. Kataeva, R. A. Cherkasov, *Phosphorus, Sulfur. Relat. Elem.* **2016**, *191*, 1576.
[2] M. R. StJ. Foreman, J. Novosad, A. M. Z. Slawin, J. D. Woollins, *J. Chem. Soc. Dalton Trans.* **1997**, 1347.
[3] M. R. StJ. Foreman, A. M. Z. Slawin, J. D. Woollins, *J. Chem. Soc. Chem. Commun.* **1995**, *2217*, 2217.
[4] M. R. StJ. Foreman, A. M. Z. Slawin, J. D. Woollins, *Chem. Commun.* **1997**, 855.
[5] M. R. StJ. Foreman, A. M. Z. Slawin, J. D. Woollins, *Chem. Commun.* **1997**, 1269.
[6] A. Dimitrov, I. Hartwich, P. Neubauer, M. Meisel, *Eur. J. Inorg. Chem.* **2004**, *2004*, 3842.
[7] E. G. Sağlam, E. Bulat, H. Yılmaz, *J. Turk. Chem. Soc. Sect. A: Chem.* **2020**, *7*, 789.
[8] I. Thomsen, K. Clausen, S. Scheibye, *Organic Synth.* **1984**, *62*, 158.
[9] G. Lajoie, F. Lépine, L. Maziak, B. Belleau, *Tetrahedron Lett.* **1983**, *24*, 3815.
[10] M. Yokoyama, Y. Hasegawa, H. Hatanaka, Y. Kawazoe, T. Imamoto, *Synthesis* **1984**, *1984*, 827.
[11] P. Wipf, C. Jenny, H. Heimgartner, *Helv. Chim. Acta* **1987**, *70*, 1001.
[12] A. Cortés-Santiago, A. M. Navarrete-López, R. Vargas, J. Garza, *J. Phys. Org. Chem.* **2017**, *30*, e3624.
[13] P. E. Newallis, J. P. Chupp, L. C. D. Groenweghe, *J. Org. Chem.* **1962**, *27*, 3829.
[14] L. Maier, *Helv. Chim. Acta* **1963**, *46*, 1812.
[15] M. R. S. J. Foreman, A. M. Z. Slawin, J. D. Woollins, *J. Chem. Soc. Dalton Trans.* **1996**, 3653.
[16] G. Ohms, U. Fleischer, V. Kaiser, *J. Chem. Soc. Dalton Trans.* **1995**, 1297.
[17] G. Ohms, A. Treichler, G. Grossmann, *Phosphorus, Sulfur. Relat. Elem.* **1989**, *45*, 95.
[18] A. Kumar, K. R. Sharma, S. K. Pandey, *Phosphorus, Sulfur Silicon Relat. Elem.* **2007**, *182*(5), 1023.
[19] H.-L. Liu, H.-Y. Mao, C. Xu, H.-Y. Zhang, H.-W. Hou, Q.-A. Wu, Y. Zhu, B.-X. Ye, L.-J. Yuan, *Polyhedron* **2004**, *23*, 1799.
[20] E. G. Sağlam, N. Acar, B. Mougang-Soumé, H. Dal, T. Hökelek, *Phosphorus, Sulfur. Relat. Elem.* **2016**, *191*, 22.

[21] V. Kabra, S. Mitharwal, S. Singh, *Phosphorus, Sulfur. Relat. Elem.* **2009**, *184*, 2431.
[22] G. M. Kishore, D. M. Shah, *Annu. Rev. Biochem.* **1988**, *57*, 627.
[23] A. Amir, A. H. Sayer, A. Ezra, B. Fischer, *Inorg. Chem.* **2013**, *52*, 3133.
[24] I. Y. Fleitlikh, N. A. Grigorieva, O. A. Logutenko, *Solvent Extr. Ion Exch.* **2018**, *36*, 1.
[25] M. Jafari, S. Chehreh Chelgani, S. Z. Shafaie, H. Abdollahi, E. Hadavandi, *J. Ind. Eng. Chem.* **2019**, *78*, 36.
[26] N. Tercero, D. R. Nagaraj, R. Farinato, *Min. Metall. Explor.* **2019**, *36*, 99.
[27] T. Dang, I. S. Nizamov, R. Z. Salikhov, L. R. Sabirzyanova, V. V. Vorobev, T. I. Burganova, M. M. Shaidoullina, E. S. Batyeva, R. A. Cherkasov, T. I. Abdullin, *Bioorg. Med. Chem.* **2019**, *27*, 100.
[28] I. S. Nizamov, T. G. Belov, I. D. Nizamov, Y. N. Nikitin, G. R. Akhmedova, O. V. Shilnikova, I. D. Timushev, R. Z. Salikhov, M. P. Shulaeva, O. K. Pozdeev, E. S. Batyeva, R. A. Cherkasov, *Phosphorus, Sulfur. Relat. Elem.* **2021**, *196*, 431.
[29] E. G. Sağlam, S. Akkoç, Y. Zorlu, E. Bulat, A. Akgün, *Polyhedron* **2021**, *199*, 115097.
[30] H. P. S. Chauhan, A. Bakshi, S. Bhatiya, *Appl. Organomet. Chem.* **2010**, *24*, 317.
[31] A. Rotar, A. Silvestru, C. Silvestru, J. E. Drake, M. B. Hursthouse, M. E. Light, L. Bunaciu, P. Bunaciu, *Appl. Organomet. Chem.* **2005**, *19*, 555.
[32] S. Bhatiya, H. P. S. Chauhan, N. Carpenter, *Appl. Organomet. Chem.* **2018**, *32*, e4026.
[33] E. Mkumbuzi, W. E. van Zyl, *J. Mol. Struct.* **2021**, *1226*, 129338.
[34] M. N. Pillay, J.-H. Liao, C. W. Liu, W. E. van Zyl, *Inorg. Chem.* **2019**, *58*, 7099.
[35] G. E. Ayom, M. D. Khan, T. Ingsel, W. Lin, R. K. Gupta, S. J. Zamisa, W. E. van Zyl, N. Revaprasadu, *Chem. A Eur. J.* **2020**, *26*, 2693.
[36] I. Haiduc, *Appl. Organomet. Chem.* **2007**, *21*, 476.
[37] W. E. van Zyl, J. D. Woollins, *Coord. Chem. Rev.* **2013**, *257*, 718.
[38] T. L. Yusuf, T. W. Quadri, G. F. Tolufashe, L. O. Olasunkanmi, E. E. Ebenso, W. E. van Zyl, *RSC Adv.* **2020**, *10*, 41967.
[39] M. R. J. Elsegood, C. R. Miles, S. J. Sharp, M. B. Smith, M. Karakus, *J. Org. Chem.* **2021**, *935*, 121668.
[40] T. L. Yusuf, C. U. Ibeji, W. E. van Zyl, *J. Mol. Struct.* **2020**, *1218*, 128517.
[41] I. S. Nizamov, A. A. Yakovlev, I. D. Nizamov, D. A. Terenzhev, K. A. Ivshin, O. N. Kataeva, M. P. Shulaeva, O. K. Pozdeev, E. S. Batyeva, R. A. Cherkasov, *Appl. Organomet. Chem.* **2018**, *32*, e4320.
[42] A. Saadat, A. Banaee, P. McArdle, K. Zare, K. Gholivand, A. A. E. Valmoozi, *J.Chem. Sci.* **2014**, *126*, 1125.
[43] C. Aydemir, S. Solak, G. Acar Doganlı, T. Sensoy, D. Arar, N. Bozbeyoglu, N. Mercan Dogan, P. Lönnecke, E. Hey-Hawkins, M. Sekerci, M. Karakus, *Phosphorus, Sulfur, Relat. Elem.* **2015**, *190*, 300.
[44] B. K. Keppler, C. Silvestru, I. Haiduc, *Met.-Based Drugs* **1994**, *1*, 73.
[45] B. Brian C. Froehler, C.A., **1993**, US 5, 194, 599 A.
[46] B. Brian C. Froehler, C.A., **2004**, US 6,756,496 B1.
[47] W. Feng, X. Y. Teo, W. Novera, P. M. Ramanujulu, D. Liang, D. J. Huang, P. K. Moore, L. W. Deng, B. W. Dymock, *J. Med. Chem.* **2015**, *58*, 6456.
[48] X.-b. Yang, Methods and compositions of improved modified siRNA, **2015**, US 2015/0322 431 A1.
[49] A. Lowe, M. Whittaker, P. Dieterich, M. Polywka, E. Cossimino, **2005**, WO 2005/095425 A1.
[50] S. Kumar, A. Syed, S. Andotra, R. Kaur, S. K. P. Vikas, *J. Mol. Struct.* **2018**, *1154*, 165.
[51] T. J. Ajayi, M. Shapi, *J. Mol. Struct.* **2020**, *1202*, 127254.
[52] M. Karakus, *Phosphorus, Sulfur. Relat. Elem.* **2011**, *186*, 1523.
[53] M. Karakus, Y. Aydogdu, O. Celik, V. Kuzucu, S. Ide, E. Hey-Hawkins, Z. Anorg, *Allg. Chem.* **2007**, *633*, 405.
[54] M. Karakus, H. Yilmaz, Y. Ozcan, S. Ide, *Appl. Organomet. Chem.* **2004**, *18*, 141.
[55] A. A. S. E. Khaldy, A. M. Abushanab, E. A. Alkhair, *Appl. Organomet. Chem.* **2011**, *25*, 491.
[56] H. Beckmann, G. Ohms, G. Großmann, K. Krüger, K. Klostermann, V. Kaiser, *Heteroat. Chem.* **1996**, *7*, 111.
[57] G. Grossmann, H. Beckmann, O. Rademacher, K. Krüger, G. Ohms, *J. Chem. Soc. Dalton Trans.* **1995**, *2797*, 2797.
[58] G. Kallinowski, W. Vogt, *Magn. Reson. Chem.* **1989**, *27*, 647.
[59] J. M. A. Al-Rawi, M. A. Sheat, N. Ayed, *Magn. Reson. Chem.* **1984**, *22*, 336.
[60] G. A. Gray, *J. Am. Chem. Soc.* **1971**, *93*, 2132.
[61] M. Karakus, H. Yilmaz, E. Bulak, P. Lönnecke, *Appl. Organomet. Chem.* **2005**, *19*, 396.
[62] R. Biswas, S. Khirid, M. Saha, C. W. Liu, R. S. Dhayal, K. K. Haldar, *Appl. Organomet. Chem.* **2019**, *33*, e5220.
[63] L. Yang, D. R. Powell, R. P. Houser, *Dalton Trans.* **2007**, 955.
[64] V. G. Albano, M. C. Aragoni, M. Arca, C. Castellari, F. Demartin, F. A. Devillanova, F. Isaia, V. Lippolis, L. Loddo, G. Verani, *Chem. Commun.* **2002**, 1170.
[65] I. P. Gray, H. L. Milton, A. M. Z. Slawin, J. D. Woollins, *Dalton Trans.* **2003**, 3450.
[66] T. J. Ajayi, M. Ollengo, L. le Roux, M. N. Pillay, R. J. Staples, S. M. Biros, K. Wenderich, B. Mei, W. E. van Zyl, *ChemistrySelect* **2019**, *4*, 7416.
[67] E. G. Sağlam, A. Ebinç, C. T. Zeyrek, H. Ünver, T. Hökelek, *J. Mol. Struct.* **2015**, *1099*, 490.
[68] Y. Ozcan, S. Ide, M. Karakuş, H. Yilmaz, *Japan Society for Analytical Chem.* **2002**, *18*, 1285.
[69] M. C. Aragoni, M. Arca, F. A. Devillanova, M. B. Hursthouse, S. L. Huth, F. Isaia, V. Lippolis, A. Mancini, S. Soddu, G. Verani, *Dalton Trans.* **2007**, 2127.
[70] I. P. Gray, A. M. Z. Slawin, J. D. Woollins, *Dalton Trans.* **2004**, 2477.
[71] M. Arca, A. Cornia, F. A. Devillanova, A. C. Fabretti, F. Isaia, V. Lippolis, G. Verani, *Inorg. Chim. Acta* **1997**, *262*, 81.
[72] M. C. Aragoni, M. Arca, F. Demartin, F. A. Devillanova, C. Graiff, F. Isaia, V. Lippolis, A. Tiripicchio, G. Verani, *Dalton Trans.* **2001**, 2671.
[73] M. C. Aragoni, M. Arca, N. R. Champness, M. de Pasquale, F. A. Devillanova, F. Isaia, V. Lippolis, N. S. Oxtoby, C. Wilson, *CrstEngComm* **2005**, *7*, 363.
[74] M. C. Aragoni, M. Arca, M. Crespo, F. A. Devillanova, M. B. Hursthouse, S. L. Huth, F. Isaia, V. Lippolis, G. Verani, *CrstEngComm* **2007**, *9*, 873.

[75] M. C. Aragoni, M. Arca, S. J. Coles, M. Crespo Alonso, S. L. Coles, R. P. Davies, M. B. Hursthouse, F. Isaia, R. Lai, V. Lippolis, *CrstEngComm* **2016**, *18*, 5620.
[76] T. Koopmans, *Physica* **1934**, *1*, 104.

SUPPORTING INFORMATION

Additional supporting information can be found online in the Supporting Information section at the end of this article.

How to cite this article: E. Bulat, E. G. Sağlam, C. T. Zeyrek, S. Akkoç, Y. Zorlu, H. Dal, *Appl Organomet Chem* **2022**, *36*(10), e6821. https://doi.org/10.1002/aoc.6821